

**Residual Stress Reduction During Quenching of Wrought 7075 Aluminum Alloy**

by

Ian Mitchell

A Master's Thesis

Submitted to the Faculty

of

WORCESTER POLYTECHNIC INSTITUTE

*in partial fulfillment of the requirements for the*

Degree of Master of Science

in

Materials Science and Engineering

May 2004

APPROVED:

---

Richard D. Sisson Jr., Advisor  
Professor of Mechanical Engineering  
Materials Science and Engineering Program Head

## **ABSTRACT**

The finite difference method was used to calculate the variable heat transfer coefficient required to maximize mechanical properties of heat treated wrought 7075 aluminum alloy without causing residual stress. Quench simulation enabled determination of maximum surface heat flux bordering on inducing plastic flow in the work piece. Quench Factor Analysis was used to correlate cylinder diameter to yield strength in the T73 condition. It was found that the maximum bar diameter capable of being quenched without residual stress while meeting military mechanical design minimums is 2". It was also found that the cooling rate must increase exponentially and that the maximum cooling rate needed to achieve minimum mechanical properties is well within the capability of metals heat treatment industry.

## LIST OF TABLES

|           |   | <b>Page</b> |
|-----------|---|-------------|
| Table 2.1 | Design Mechanical Properties of 7075 Aluminum Alloy,<br>Die Forging           | 4           |
| Table 2.2 | Effects of Part Temperature and Quench Temperature on<br>Residual Stress      | 14          |
| Table 2.3 | Effect of Quenchant Temperature and Agitation on Heat<br>Transfer Coefficient | 16          |

## LIST OF FIGURES

|             |   | Page |
|-------------|---|------|
| Figure 2.1  | Precipitation Rate v. Temperature   | 5    |
| Figure 2.2  | AA7075 - C(T) Curve   | 6    |
| Figure 2.3  | Average Cooling Rates for Various Water Temperatures and Plate Thicknesses                    | 7    |
| Figure 2.4  | Effect of Cooling Rate on Tensile Strengths for Various Aluminum Alloys                       | 7    |
| Figure 2.5  | Method of Quench Factor Calculation   | 9    |
| Figure 2.6  | Maximum Attainable Properties v. Quench Factor  | 10   |
| Figure 2.7  | 7076-T6 Rod, Quenched in Cold Water and not Stress Relieved                                   | 12   |
| Figure 2.8  | Idealized Quench Curve  | 13   |
| Figure 2.9  | Effect of Quenching from 540°C (1000°F) on Residual Stresses in Solid Cylinders of Alloy 6151 | 14   |
| Figure 2.10 | Heat Transfer Coefficient v. Glycol%  | 16   |
| Figure 2.11 | Effect of Surface Condition on Cooling Curve  | 17   |
| Figure 2.12 | Finite Difference Node Diagram  | 20   |
| Figure 2.13 | Characteristic Boiling Curve  | 22   |
| Figure 3.1  | AA7075 - Poisson's Ratio v. Temperature   | 25   |
| Figure 3.2  | AA7075 - Modulus of Elasticity (Young's Modulus) v. Temperature                               | 26   |
| Figure 3.3  | AA7075 - Thermal Conductivity v. Temperature  | 26   |
| Figure 3.4  | AA7075 - Specific Heat v. Temperature   | 27   |
| Figure 3.5  | AA7075 - Coefficient of Thermal Expansion v. Temperature                                      | 27   |
| Figure 3.6  | AA7075 - Density v. Temperature   | 28   |
| Figure 3.7  | Nodal Cooling Curve, Ø2" Bar, at Elasticity Limit   | 30   |
| Figure 3.8  | Chasing Elasticity Limit with Thermal Stress  | 31   |
| Figure 3.9  | Elastic Limit Heat Transfer Coefficients v. Time  | 32   |
| Figure 3.10 | Elastic Limit Quench Factor v. Bar Diameter   | 33   |
| Figure 3.11 | Elastic Limit Yield Strength v. Bar Diameter  | 33   |
| Figure 3.12 | Boiling Water Quench Simulation   | 35   |
| Figure 3.13 | Room Temperature Quench Simulation  | 35   |
| Figure 4.1  | Program Flowchart   | 38   |

## TABLE OF CONTENTS

|  | <b>Page</b> |
|--|-------------|
| ABSTRACT   | i           |
| LIST OF TABLES   | ii          |
| LIST OF FIGURES  | iii         |
| <b>1.0</b> INTRODUCTION                                  | 1           |
| <b>2.0</b> LITERATURE REVIEW                             | 3           |
| <b>2.1.</b> Quenching                                    | 4           |
| <b>2.2.</b> Residual Stress                              | 11          |
| <b>2.3.</b> Thermal Stress                               | 18          |
| <b>3.0</b> PROCEDURE                                     | 24          |
| <b>4.0</b> PROGRAM DESCRIPTION                           | 36          |
| <b>5.0</b> CONCLUSIONS                                   | 38          |
| <b>6.0</b> RECOMMENDATIONS FOR FUTURE WORK               | 39          |
| <b>7.0</b> APPENDIX A – STRESS EQUATION DERIVATIONS      | 41          |
| <b>8.0</b> APPENDIX B – TEMPERATURE EQUATION DERIVATIONS | 43          |
| <b>9.0</b> APPENDIX C – MATLAB PROGRAM                   | 44          |
| <b>10.0</b> REFERENCES                                   | 48          |

## 1.0 INTRODUCTION

The aerospace industry relies heavily on aluminum alloy forgings because they exhibit high strength-to-weight-to-cost properties. Aluminum alloy 7075, in particular, has one of the highest attainable strength levels of all forged alloys and is capable of good stress corrosion resistance. For these reasons, aerospace engineers have historically preferred to specify 7075 aluminum forgings in the T73 temper for components used in helicopters, airplanes and ordnance.

Alloy 7075 has a major shortcoming among other 7xxx series alloys. Its superb heat-treated mechanical properties depend on high quench rates to maximize the artificial aging (precipitation hardening) response. High quench rates, however, cause thermal stresses to develop that can exceed the instantaneous local yield strength. In these cases, tensile plastic flow occurs at the part surface where stresses are highest. Upon full cooling, the part exhibits compressive surface stress balanced by tensile core stress.

Normally, compressive surface stress is desirable in terms of resistance to fatigue and stress corrosion. Unfortunately, the likely subsequent machining operation not only removes the surface condition, but can result in dimensional stability problems. As the compressive surface layer is removed, the internal static equilibrium is disrupted and the part distorts from its heat-treated shape. This warping potentially leads to scrapped parts or added rework, both of which add to the overall manufactured cost of the part.

Methods exist for reducing the magnitude of plastic flow while maintaining the required quench rate and for mitigating the effects of plastic flow after the quench. Most of the methods involve adding manufacturing cost and/or complexity to a process that could potentially be accomplished through a controlled quench process using only air and

water, and without added handling or processing. A question remains unanswered: What are the theoretical physical limits of performing a successful quench without incurring plastic flow?

The goal of this thesis is to calculate, for several diameters of aluminum alloy 7075 bar, the maximum allowable quench rates short of inducing plastic flow. The importance lies in finding the maximum cooling rate curve that provides sufficient quench rate without inducing residual stress, and in finding the maximum bar diameter corresponding to minimum property levels.

## **2.0 LITERATURE REVIEW**

Aluminum alloys fall into two general categories: heat-treatable and non-heat-treatable. Series 7xxx alloys, considered the high strength aircraft alloy family, are heat-treatable by solution and aging. Various aging cycles produce desired attributes such as maximum attainable strength (T6 temper) or stress corrosion resistance (T73 temper). Either way, the alloy must go through solution treatment, the goal of which is to completely dissolve into solid solution all alloy elements responsible for subsequent precipitation hardening. After achieving complete solution, the alloy must be quenched quickly enough to effectively freeze the solid solution so that maximum supersaturation is achieved at room temperature. [1] This process sets the stage for precipitation hardening.

Alloy 7075, with nominal composition [2] of 5.6% Zn, 2.5% Mg, 1.6% Cu, 0.3% Cr, has one of the highest attainable strengths of all aluminum alloys. Military design strengths (minimum mechanical properties) for die forgings (with maximum attainable strengths) are partially listed in Table 2.1.

**Table 2.1- Design Mechanical Properties of 7075 Aluminum Alloy, Die Forging [2,3]**

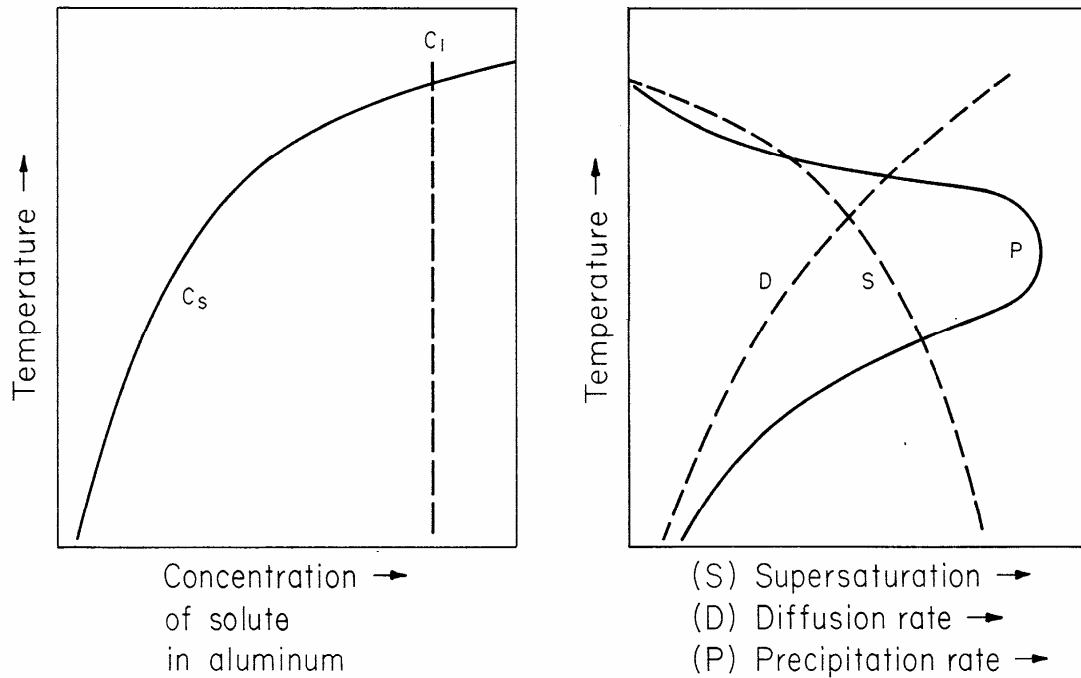
| <b>TEMPER</b> | <b>SECTION THICKNESS</b>  | <b>TENSILE STRENGTH</b> | <b>YIELD STRENGTH</b> |
|---------------|---------------------------|-------------------------|-----------------------|
| T6            | <i>maximum attainable</i> | <i>83,000 psi</i>       | <i>73,000</i>         |
|               | Up through 1”             | 75,000                  | 64,000                |
|               | Over 1 through 3          | 74,000                  | 63,000                |
|               | Over 3 through 4          | 73,000                  | 62,000                |
| T73           | <i>maximum attainable</i> | <i>73,000 psi</i>       | <i>63,000</i>         |
|               | Up through 3              | 66,000                  | 56,000                |
|               | Over 3 through 4          | 64,000                  | 55,000                |

## **2.1 QUENCHING**

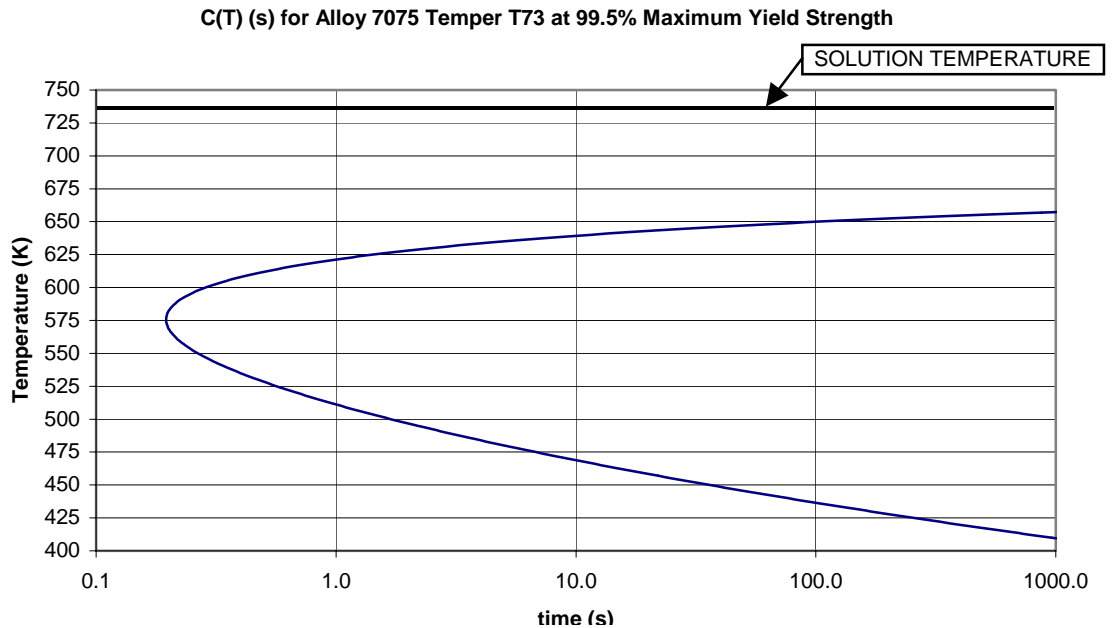
As can be seen in Table 2.1, design strength decreases as section thickness increases. Alloy 7075 is highly quench rate sensitive in this regard. The maximum attainable strengths coincide with maximum cooling rate. As the cooling rate decreases, more time is allowed for solute to come out of solution and precipitate at grain boundaries. If the quench rate is sufficiently slow, precipitation can occur intragranularly. Both conditions reduce the precipitation hardening response. The existence of atomic vacancies in the as-quenched condition (designated temper W) also contributes to aging response. These vacancies bolster the precipitation hardening response by providing nucleation sites for homogeneous precipitation. Slow quenching allows vacancies to diffuse with great rapidity to disordered areas thus negatively affecting the spacing and quantity of nucleation sites and the resultant mechanical properties. [1]

Figure 2.1 illustrates how precipitation rates vary with temperature. At temperatures near melting, diffusion rates are high but the alloying elements exhibit high solubility, so that precipitation is non-existent. At room temperature, diffusion rates and

solubility are low, so that precipitation proceeds very slowly. At mid-range temperatures, precipitation is rapid because diffusion rates, and the driving force for precipitation, are moderate and combine to drive elements out of solution. Rapid cooling through the mid-temperature range is critical in preventing supersaturation loss. For a given alloy and property combination, a time-temperature-property curve (C-curve) might be constructed as in Figure 2.2. The idea is similar to the classic time-temperature-transformation curve used for predicting the properties of heat-treated steel alloys.



**Figure 2.1 - Precipitation Rate v. Temperature [4]**



**Figure 2.2 – AA7075 - C(T) Curve**

The solution cycle for alloy 7075 forgings consists of heating to 880F and holding at that temperature for approximately one hour per inch of diameter. This amount of time at temperature assures that sufficient diffusion has occurred to allow complete solution of alloying elements. The temperature is held just below the eutectic melting point to maximize diffusion rate and solubility. The critical cooling range is generally accepted at 750F to 550F. Figure 2.3 shows calculated average cooling rates through this critical temperature range for various water quench temperatures and plate thicknesses. Correlations exist between average cooling rates through the critical range and properties in the aged condition. For example, Figure 2.4 below shows correlation of average cooling rate with tensile strength for various alloys. These correlations, however, are only approximate because property variations exist between thick and thin sections of material with equivalent average cooling rates, and because precipitation can occur outside this critical temperature range. [1] A method known as Quench Factor Analysis was devised by Evancho and Staley [5] to improve property prediction accuracy.

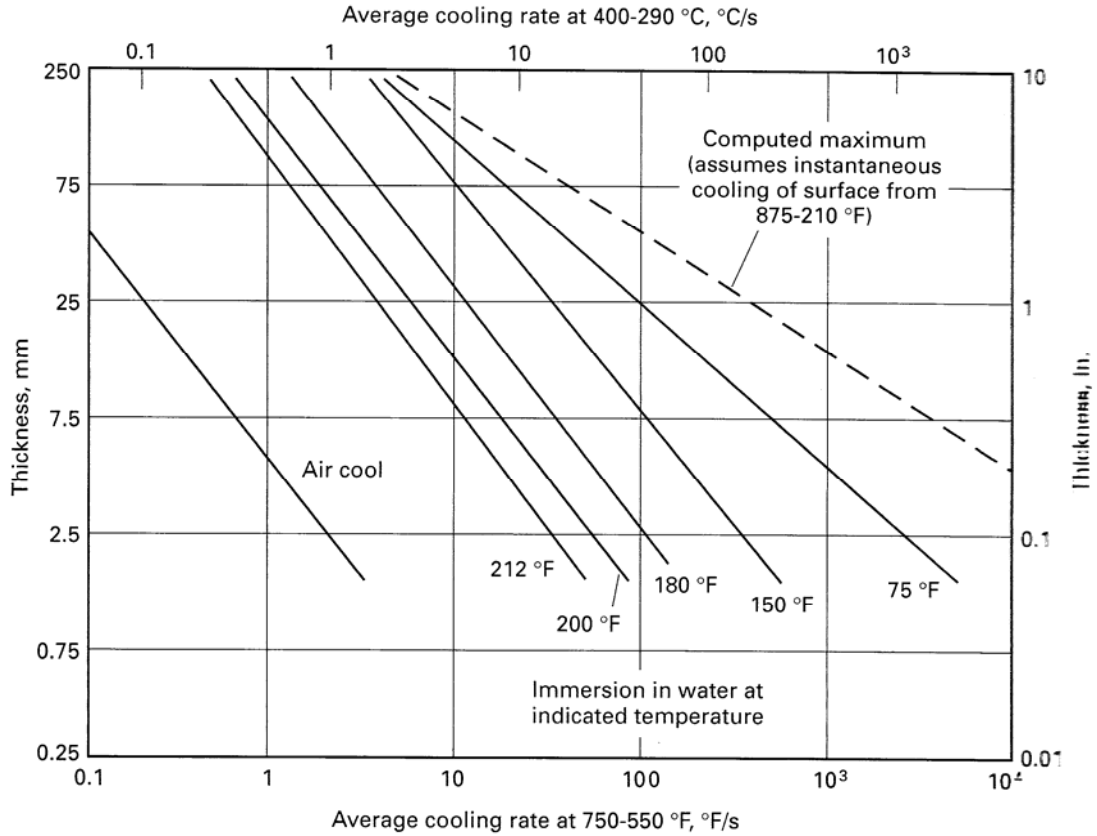


**Figure 2.3 – Average Cooling Rates for Various Water Temperatures and Plate Thicknesses [4]**

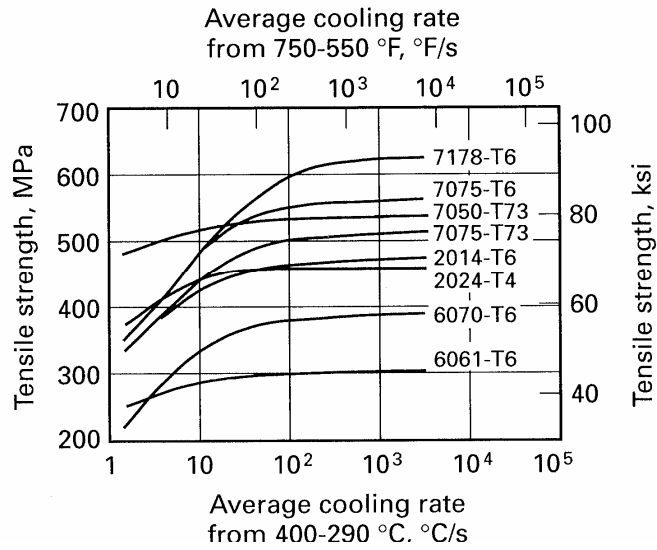


**Figure 2.4 – Effect of Average Cooling Rate on Tensile Strengths for Various Aluminum Alloys [1]**

Quench Factor Analysis (QFA) takes into account the entire continuous cooling curve to predict properties. Predictions are based on precipitation kinetics during the quench that may be described by

$$\xi = 1 - \exp(k_1 \tau)$$

where  $\xi$  is the fraction untransformed,

$k_1 = \ln(\text{fraction untransformed during quench, usually 99.5\%}) = -0.005013$ , and

$$\tau = \int_{t_0}^{t_f} \frac{dt}{C(T)}$$

where  $t$  is time (seconds),

$t_0 = 0$  at start of quench,  $t_f =$  time elapsed by end of quench,  $C(T)$  is the temperature dependent time value on the C-curve, and  $\tau$  is the quench factor.

The C-curve may be described by the following equation:

$$C(T) = -k_1 k_2 \exp\left[\frac{k_3 k_4^2}{RT(k_4 - T)^2}\right] \exp\left[\frac{k_5}{RT}\right]$$

where  $C(T)$  is the critical time required to precipitate a constant amount of solute (s),

$k_1$  is the same as above (-0.005013)

$k_2$  is a constant related to the reciprocal of the number of nucleation sites (s)

$k_3$  is a constant related to the energy required to form a nucleus (J/mol)

$k_4$  is a constant related to the solvus temperature (K)

$k_5$  is a constant related to the activation energy for diffusion (J/mol)

$R =$  gas constant (8.31441 J/mol-K)

$T =$  temperature (K)

By knowing the cooling curve and property-specific C-curve,  $\tau$  may be integrated

by summation:

$$\tau = \sum \frac{\Delta t}{C(T)}$$

as illustrated in Figure 2.6.

Knowing  $\tau$  allows property prediction by the following equation:

$$P = P_{\max} \exp(k_1 \tau)$$

where  $P$  is the property of interest and  $P_{\max}$  is the maximum attainable value of  $P$ . The

Figure 6 shows how  $P$  as a percentage of  $P_{\max}$  varies with  $\tau$ .

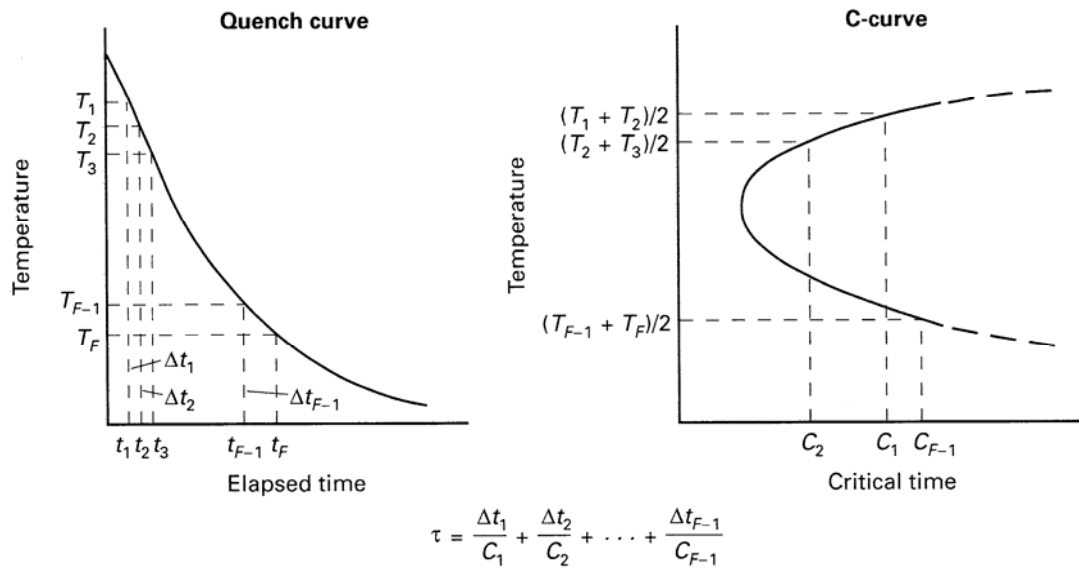


**Figure 2.5 – Method of Quench Factor Calculation [5]**

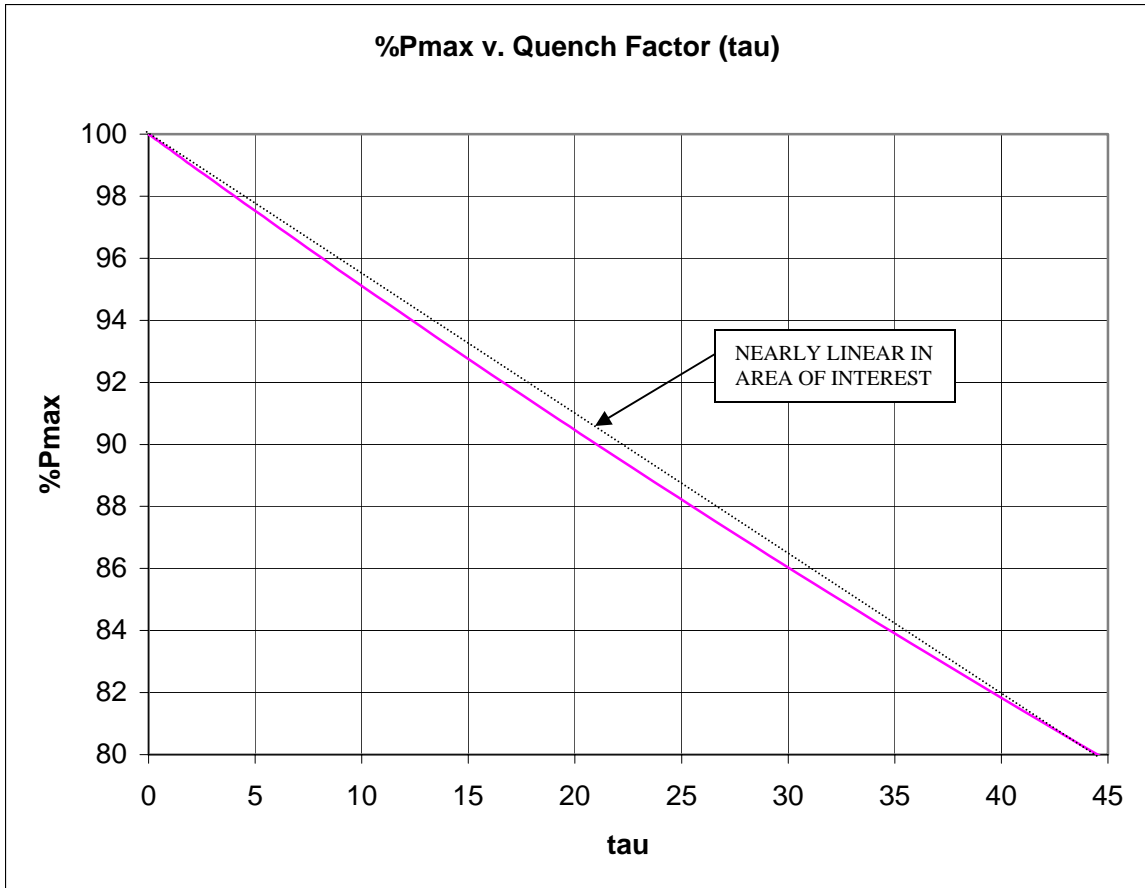


**Figure 2.6 - Maximum Attainable Property v. Quench Factor**

The constants that define the C-curve for alloy 7075 in the T73 condition (Figure 2.2) are [6]:

$$k_2 = 1.37E-13 \text{ s}$$

$$k_3 = 1069 \text{ J/mol}$$

$$k_4 = 737\text{K}$$

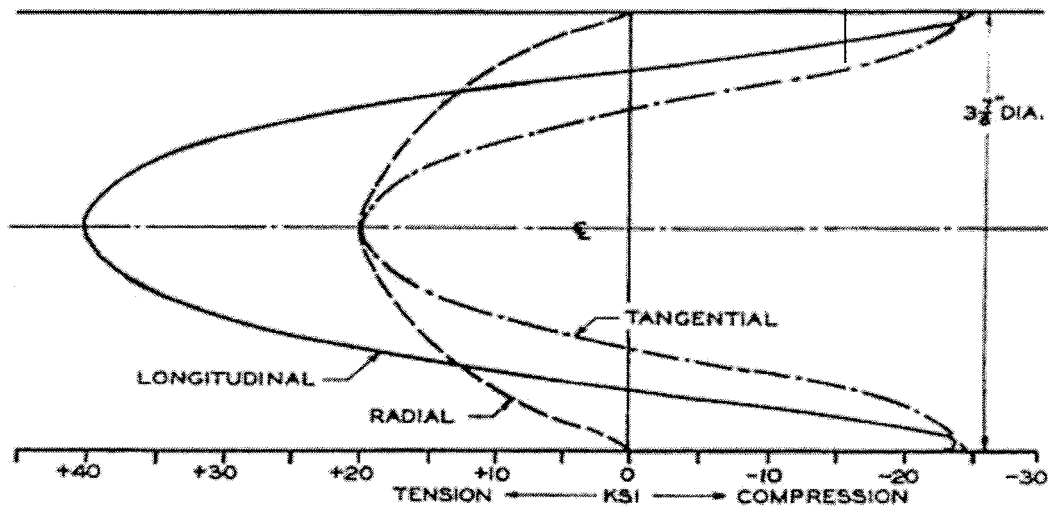
$$k_5 = 137000 \text{ J/mol}$$

## 2.2 RESIDUAL STRESS

Unfortunately, in industrial practice, cooling rates required to achieve minimum design strengths listed in Figure 2.1 induce thermal stresses (due to differential thermal contraction) far greater than yield strength. When thermal stresses exceed yield strength, localized plastic flow occurs resulting in the work piece exhibiting a state of residual stress at room temperature. [7]

Residual stress is problematic in several ways. It may cause permanent distortion beyond acceptable dimensional tolerance limits. It may also cause the work piece to distort during machining operations. Either way, the potential exists for producing scrap or rework, both of which add to overall manufactured cost. Moreover, a compressive surface stress state can be beneficial to resistance to both fatigue and stress corrosion. If the surface is subsequently machined away to expose the underlying tensile stress state, these benefits may be compromised or reversed. If the surface is allowed to become tensile, parts may fail in service in a shorter time than expected. [7]

Just prior to quenching, yield strength is very low because temperature is close to the eutectic melting point. Even a small amount of thermal stress at this temperature can cause plastic flow. During the quench, the surface naturally cools earlier than the interior. The cooler surface tries to thermally contract but is resisted by the warmer interior. This places the surface in a state of tension and the interior in a state of compression. Under sufficient thermal stress, the surface will yield in tension. Then, as the center cools and contracts, it tries to pull in the cooler, stronger, stretched surface. The stress states reverse, and upon full cooling, the surface will be in compression and the interior in tension [7] as Figure 2.7 illustrates.



**7075-T6 ROD, QUENCHED IN COLD WATER AND NOT STRESS RELIEVED**  
**Figure 2.7**

Source: NASA-STD-6004 (P025) May 21, 2002

There are two ways to deal with residual stress: by mitigation through an added operation after residual stress has been imparted and by controlling the quench parameters. Because the thrust of this thesis pertains to avoidance of residual stress, only the quenching aspect will be considered.

Consider the idealized quench curve shown in Figure 2.8. The region of yielding and residual stress development occurs at the beginning of the quench when thermal gradients are highest and yield strengths are lowest. The critical range does not necessarily overlap the region of yielding. Cooling rates in the critical range may be high without yielding because the yield strength has increased with decreased temperature. Finally, at low temperatures, the quench rate has an insignificant effect on the quench factor. Control of the quench process parameters affords the heat treater with opportunities to reduce the magnitude of yielding or even avoid it altogether. Keep in

mind that, in general, reduced quench severity means reduced cooling rate and reduction in properties, and that minimum properties must always be met.

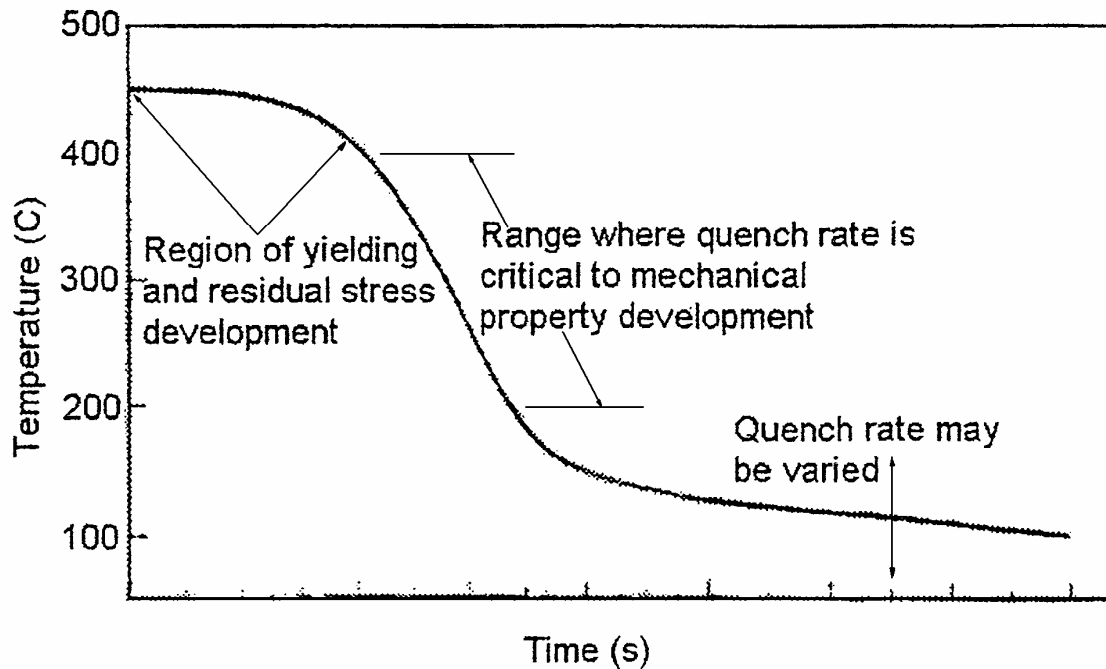
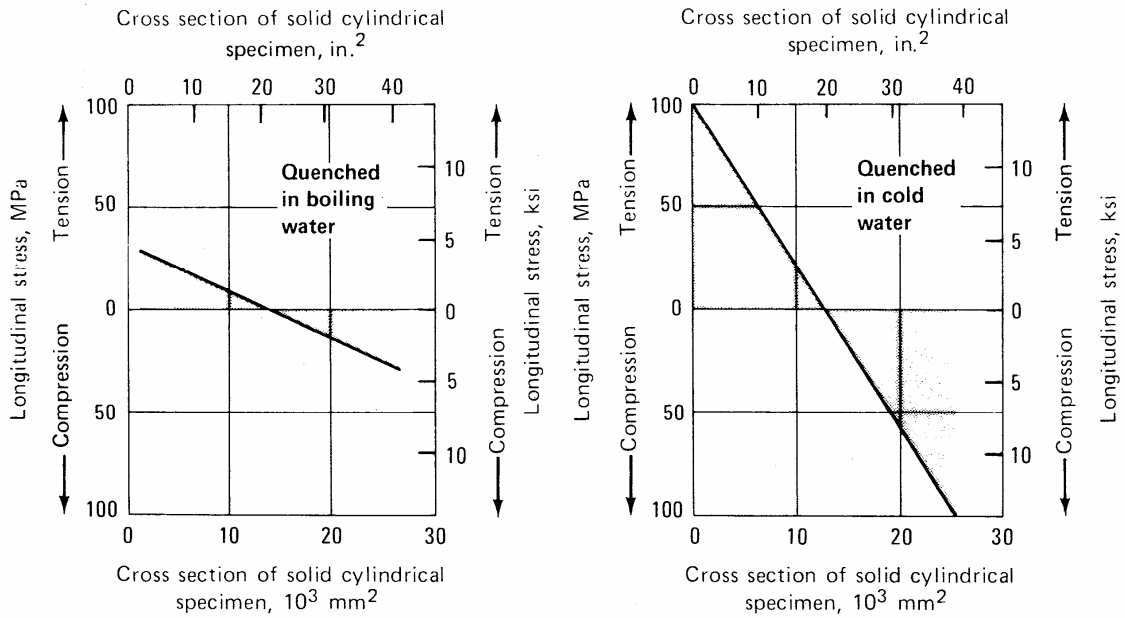


**Figure 2.8 – Idealized Quench Curve [8]**

Water temperature adjustment is by far the easiest method of reducing quench severity. Figure 2.3 illustrates the average cooling rate trend and Figure 2.9 is a comparison of residual stresses developed in different water quench temperatures. Table 2.3 shows how heat transfer coefficient varies with quenchant temperature. Standard quench practice for alloy 7075 employs agitated water at 140-160F. [1] The temperature of the work piece at the time of quench may also be adjusted easily by slow cooling in the furnace to the desired temperature. Recent work has shown that mechanical properties remain high when parts are allowed to cool to a temperature that would not provide complete solutionizing prior to quench. This is possible because the effects of the C-curve, especially for 7075-T73, begin at temperatures well below the required solution

temperature. Residual stresses decrease because the yield strength at these lower temperatures is higher than at the standard solution temperature. Table 2.2 shows the relative magnitude of residual stresses for various combinations of water temperature and part temperature. Note that not only does quenchant temperature affect residual stress, but so does the part temperature at the start of quench.



Effect of quenching from 540 °C (1000 °F) on residual stresses in solid cylinders of alloy 6151

Figure 2.9 [1]

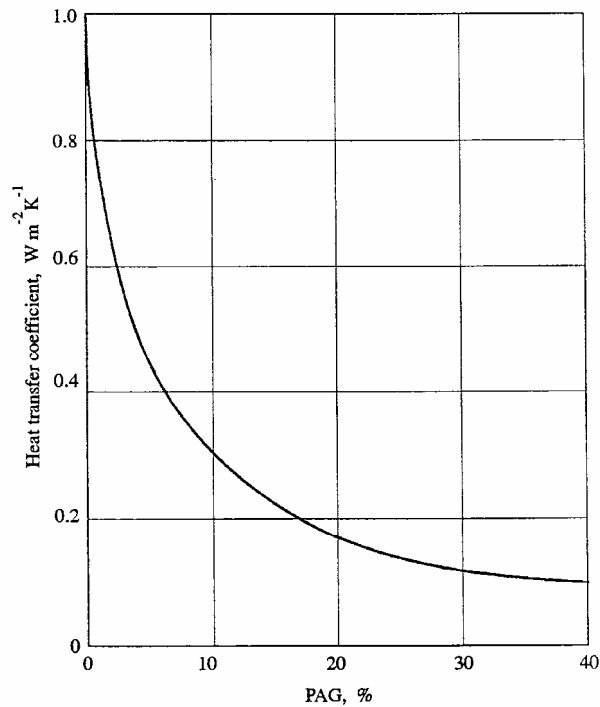
| Quench           | Residual Stress MPa | % Reduction in RS | Rp <sub>0.2</sub> MPa |
|------------------|---------------------|-------------------|-----------------------|
| 475°C-RT         | -149±11             |                   | 448                   |
| 475°C-75°C       | -65±13.3            | 56%               | 438                   |
| 475°C-450°C-RT   | -139±7.7            | 7%                | 449                   |
| 475°C-450°C-75°C | -22±11.5            | 85%               | 432                   |
| 475°C-425°C-RT   | -126±8.7            | 15%               | 446                   |
| 475°C-425°C-75°C | -17.3±8.9           | 89%               | 439                   |

Table 2.2 – Effect of Part Temperature and Quench Temperature on Residual Stress [9]

A quench process may benefit from additions of glycol to water. The glycol effectively forms a film at the part surface when immersed in the quenchant and breaks down at an engineered temperature. This allows the part to cool slowly at first due to the film's low heat transfer rate and then increase to a rate suitable for attainment of minimum properties. Figure 2.10 shows how the average heat transfer coefficient through the critical range of 700-530K varies with percent glycol. Additions of glycol are effective but the percent by volume ratio must be maintained within specified limits. Maintenance of the glycol ratio is required because as work is pulled from the quench bath (and subsequently rinsed) the glycol sticks to the parts. This effect is called dragout and it causes the glycol ratio to drop over time. Glycol-water quenchants also mitigate the effects of agitation level as deduced from Table 2.3. This means that the heat transfer rate to the quenchant is fairly uniform regardless of whether the quenchant is stagnant or violent. On the downside, larger cross sections will not cool quickly enough to achieve sufficient quench, and size limitations are imposed. Other quenchants such as oil and air may be used as long as minimum properties are met. [1,7]

Surface condition has a major bearing on quench rate, but is seldom used as a way to control the quench process. Figure 2.11 captures some of the effects. Usually, product is cleaned prior to any heat treat operation and thus has the slowest quench. [7]

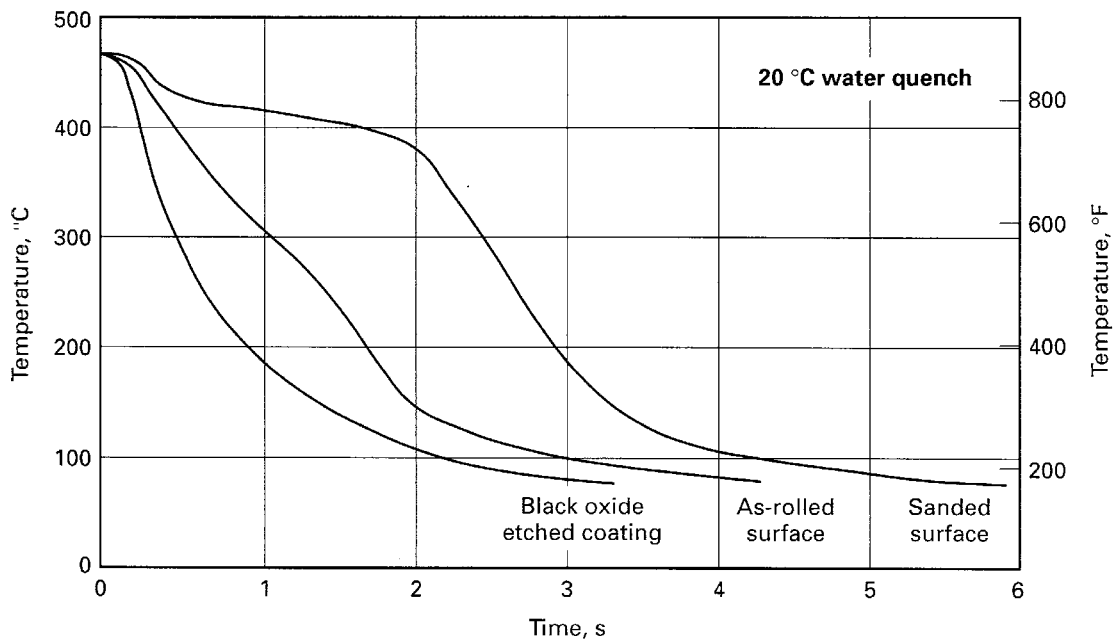
Lastly, section size can be reduced to decrease the total temperature difference from the surface to the mass center. This reduction decreases the thermal stress magnitude and thusly the level of residual stress. Care must be taken so as not to create geometry conducive to trapping air, forming areas prone to quenchant stagnation, or sharp inside corners that might create favorable distortion points. [7]



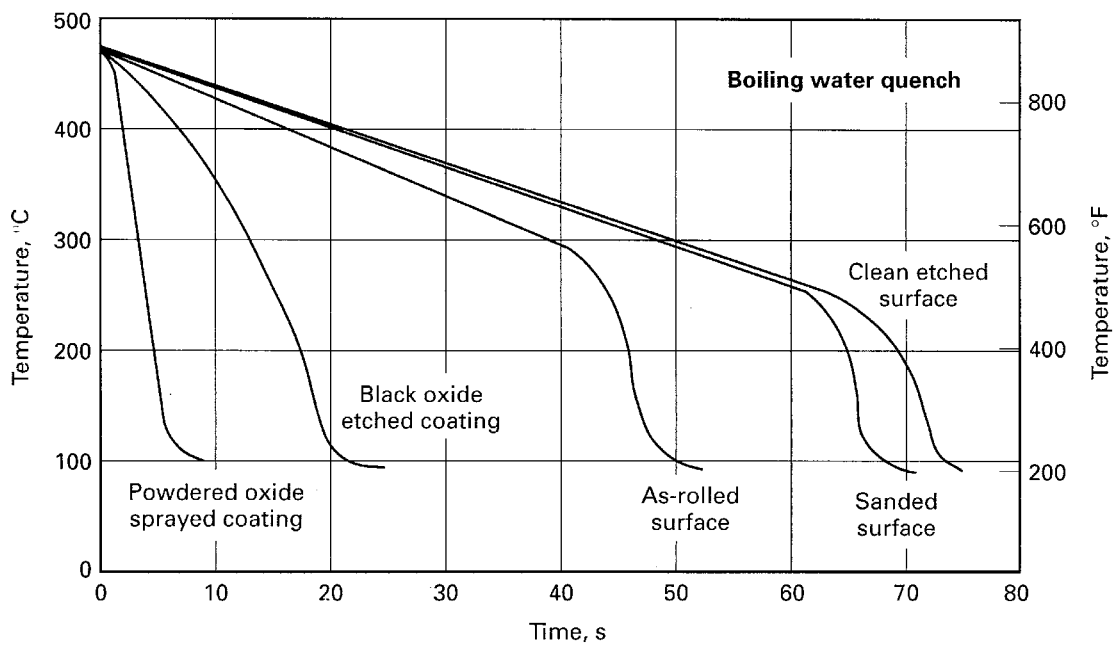
**Figure 2.10 – Heat Transfer Coefficient v. Glycol% [10]**

**Table 2.3 - Effect of Quenchant Temperature and Agitation on Heat Transfer Coefficient [8]**

| Quenchant  | Temperature (F) | Velocity (m/s) | Heat Transfer Coeff. ( $W/cm^2K$ ) | Range ( $W/cm^2K$ ) |
|------------|-----------------|----------------|------------------------------------|---------------------|
| Water      | 140             | 0.00           | 2.85                               | 1.56                |
|            |                 | 0.25           | 3.62                               |                     |
|            |                 | 0.50           | 4.41                               |                     |
| Water      | 160             | 0.00           | 0.70                               | 1.92                |
|            |                 | 0.25           | 1.89                               |                     |
|            |                 | 0.50           | 2.62                               |                     |
| Water      | 180             | 0.00           | 0.36                               | 0.53                |
|            |                 | 0.25           | 0.69                               |                     |
|            |                 | 0.50           | 0.89                               |                     |
| Water      | 200             | 0.00           | 0.20                               | 0.10                |
|            |                 | 0.25           | 0.27                               |                     |
|            |                 | 0.50           | 0.30                               |                     |
| Water      | 212             | 0.00           | 0.13                               | 0.00                |
|            |                 | 0.25           | 0.13                               |                     |
|            |                 | 0.50           | 0.13                               |                     |
| 25% UCON A | 85              | 0.00           | 0.63                               | 0.14                |
|            |                 | 0.25           | 0.70                               |                     |
|            |                 | 0.50           | 0.77                               |                     |
| 25% PVP90  | 85              | 0.00           | 1.49                               | 0.15                |
|            |                 | 0.25           | 1.34                               |                     |
|            |                 | 0.50           | 1.41                               |                     |



(a)



(b)

Effect of surface conditions on the midplane cooling of a 13 mm (0.5 in.) thick plate of 7075 from quenching in (a) 20 °C (70 °F) water and (b) boiling water.

**FIGURE 2.11 – Effect of Surface Condition on Cooling Curve [11]**

### 2.3 THERMAL STRESS

Any unrestrained body with non-zero coefficient of thermal expansion will experience thermal strain under the effect of a thermal gradient. The thermal strains that must occur to keep the body continuous induce associated thermal stresses. [12]

Transient thermal gradients may lead to thermal stresses higher than those expected under static thermal loading. Under sufficiently severe gradients, strain rate sensitivity can come into play when stress is an increasing function of strain rate. In these cases, thermal stress is considered thermal shock and static thermal stress equations must be modified to account for strain rate. Thermal shock phenomena will not be considered here.

In the elastic strain regime, stress function  $\phi$  is found from

$$\nabla^4 \phi + E\alpha \nabla^2 T = 0,$$

where E is the (constant) modulus of elasticity,  $\alpha$  is the (constant) coefficient of thermal expansion, and T is the temperature. [12] For arbitrary shapes, the exact solution to this equation is either analytically impossible or formidably cumbersome.

Some simpler shapes have exact solutions. Take, for example, the generalized plain-strain case of the infinitely long cylinder with unrestrained ends and radial temperature variation. The solution is a variant of the plane-stress case, for which the governing stress equilibrium and compatibility equations are, respectively

$$\begin{aligned} \frac{d}{dr}(r\sigma_r) - \sigma_\theta &= 0 \\ \frac{d}{dr}\left(\frac{\sigma_\theta}{E}\right) - \frac{d}{dr}\left(\frac{\mu\sigma_r}{E}\right) + \frac{d}{dr}(\alpha\Delta T) - \frac{(1+\mu)(\sigma_r - \sigma_\theta)}{Er} &= 0 \end{aligned}$$

where r is the radial dimension,  $\mu$  is Poisson's Ratio and  $\Delta T$  is the temperature increment above which there is no thermal stress. To obtain the plain-strain solution,  $E\alpha$  is replaced

by  $E\alpha/(1-\mu)$  and the zero net axial force condition is applied. If  $E$ ,  $\mu$  and  $\alpha$  are all constant, the equations may be solved directly to give

$$\begin{aligned}\sigma_r &= \frac{E\alpha}{1-\mu} \left( \frac{1}{b^2} \int_0^b T r dr - \frac{1}{r^2} \int_0^r T r dr \right) \\ \sigma_\theta &= \frac{E\alpha}{1-\mu} \left( \frac{1}{b^2} \int_0^b T r dr + \frac{1}{r^2} \int_0^r T r dr - T \right) \\ \sigma_z &= \frac{E\alpha}{1-\mu} \left( \frac{2}{b^2} \int_0^b T r dr - T \right)\end{aligned}$$

where  $b$  is the cylinder radius. [12] In reality,  $E$ ,  $\mu$  and  $\alpha$  are all variable and exact solutions may be analytically impossible. To overcome this obstacle, the finite difference method may be used to discretize the ordinary differential equations of equilibrium and compatibility into difference equations. The discretized versions of the plane-stress equations at position  $i-1/2$  become

$$\begin{aligned}\frac{r_i \sigma_{r,i} - r_{i-1} \sigma_{r,i-1}}{r_i - r_{i-1}} - \frac{\sigma_{\theta,i} + \sigma_{\theta,i-1}}{2} &= 0 \\ \frac{\sigma_{\theta,i}}{E_i} - \frac{\sigma_{\theta,i-1}}{E_{i-1}} - \frac{\mu_i \sigma_{r,i}}{E_i} + \frac{\mu_{i-1} \sigma_{r,i-1}}{E_{i-1}} + \frac{\alpha_i \Delta T_i - \alpha_{i-1} \Delta T_{i-1}}{r_i - r_{i-1}} - \\ &\quad \left[ \frac{(1 + \mu_i)(\sigma_{r,i} - \sigma_{\theta,i})}{E_i r_i} + \frac{(1 + \mu_{i-1})(\sigma_{r,i-1} - \sigma_{\theta,i-1})}{E_{i-1} r_{i-1}} \right] &= 0\end{aligned}$$

These equations can accommodate variations in physical properties with temperature, but must be solved simultaneously. [12] These equations cannot be transformed from plane-stress to plane-strain with a simple substitution as above. Rather, the compatibility equation must be derived from plain-strain conditions. The complete derivation of generalized plain-strain difference equations is contained in Appendix A.

Use of these equations requires a known temperature profile. The cross section of a cylinder may be depicted as shown in Figure 2.12 for the purpose of numerical analysis. N denotes the number of subdivisions and P (the surface node) = N + 1. Each node represents the volume of the corresponding annulus of unit length L along the cylinder.

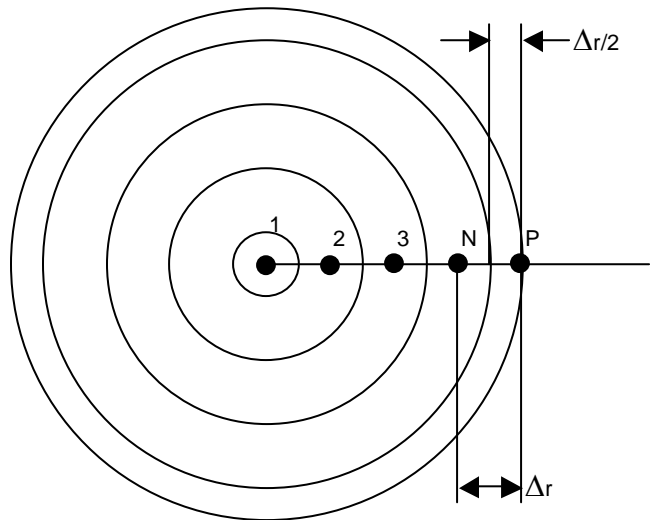


**Figure 2.12 - Finite Difference Node Diagram**

Fourier's Law of Heat Conduction in cylindrical differential form describes, for this case, the heat flux at any internal radius. The surface heat flux is described by convection. The equations are, respectively

$$q_r = -k \frac{dT}{dr}$$

$$q_s = h(T_\infty - T_s)$$

where q is the heat flux, k is thermal conductivity, dt/dr is the temperature gradient, h is the convection coefficient,  $T_s$  is the ambient temperature and  $T_\infty$  is the surface temperature. To apply these equations to any node, an energy balance is set up where Heat In – Heat Out = Heat Accumulation

The following three energy balances apply to the model at hand:

FOR INTERNAL NODES  $i$ :

$$\left( Ak \frac{dT}{dr} \right)_{i-1/2} - \left( Ak \frac{dT}{dr} \right)_{i+1/2} = \rho \left( VC_p \frac{dT}{dt} \right)_i$$

FOR AXIS NODE  $i = 1$ :

$$0 - \left( Ak \frac{dT}{dr} \right)_{3/2} = \rho \left( VC_p \frac{dT}{dt} \right)_1$$

FOR SURFACE NODE  $i = N + 1 = P$ :

$$\left( Ak \frac{dT}{dr} \right)_{P-1/2} - (AhdT)_P = \rho \left( VC_p \frac{dT}{dt} \right)_P$$

where A is the circumference times unit length,  $\rho$  is the material density, V is the unit length nodal volume,  $C_p$  is the heat capacity and  $dT/dt$  is the rate of temperature change with time. [13]

By converting to difference form, these equations may be rearranged to allow calculation of nodal temperatures at the next time increment based on the current nodal temperature of that node and any adjacent nodes. The equations are

FOR INTERNAL NODES  $i$ :

$$T_i^{t+1} = T_{i-1} \left[ \Theta^- \left( \frac{i-3/2}{i-1} \right) \right] + T_i \left[ 1 - \Theta^- \left( \frac{i-3/2}{i-1} \right) - \Theta^+ \left( \frac{i-1/2}{i-1} \right) \right] + T_{i+1} \left[ \Theta^+ \left( \frac{i-1/2}{i-1} \right) \right]$$

FOR AXIS NODE  $i = 1$ :

$$T_1^{t+1} = T_1 [1 - 4\Theta^+] + T_2 [4\Theta^+]$$

FOR SURFACE NODE  $i = N + 1 = P$ :

$$T_P^{t+1} = T_{P-1} \left[ 2\Theta^- \left( \frac{N-1/2}{N-1/4} \right) \right] + T_P \left[ 1 - 2\Theta^- \left( \frac{N-1/2}{N-1/4} \right) \right] + (T_\infty - T_P) \frac{4h\Delta t}{\rho C_p \Delta r} \left( \frac{N}{2N-1/2} \right)$$

$$\text{where } \Theta = \frac{k\Delta t}{\rho C_p (\Delta r)^2}$$

Appendix B contains complete derivations of these equations.

Heat flux and the resultant temperature profile are completely determined by material properties and surface convection. Material properties are either already known or can be determined by laboratory testing. Surface convection, on the other hand, is highly variable due to the complex nature of the quench process as depicted in Figure 2.13. The start of quench begins with Stage V cooling, and progresses to Stage I. Stage V and IV correspond with the region of yielding and residual stress development (also known as A-stage cooling), Stage IV and III with the critical cooling range (B-stage cooling), and Stage II with the final non-critical range (C-stage cooling). The real heat transfer coefficient ( $h$ ) is a complex function of surface temperature for a given quench condition. To simulate a quench process, the heat transfer coefficient function of temperature may be derived from experimental results in the form of a fitted curve. [15] At each increment, the surface temperature would dictate the heat transfer coefficient.

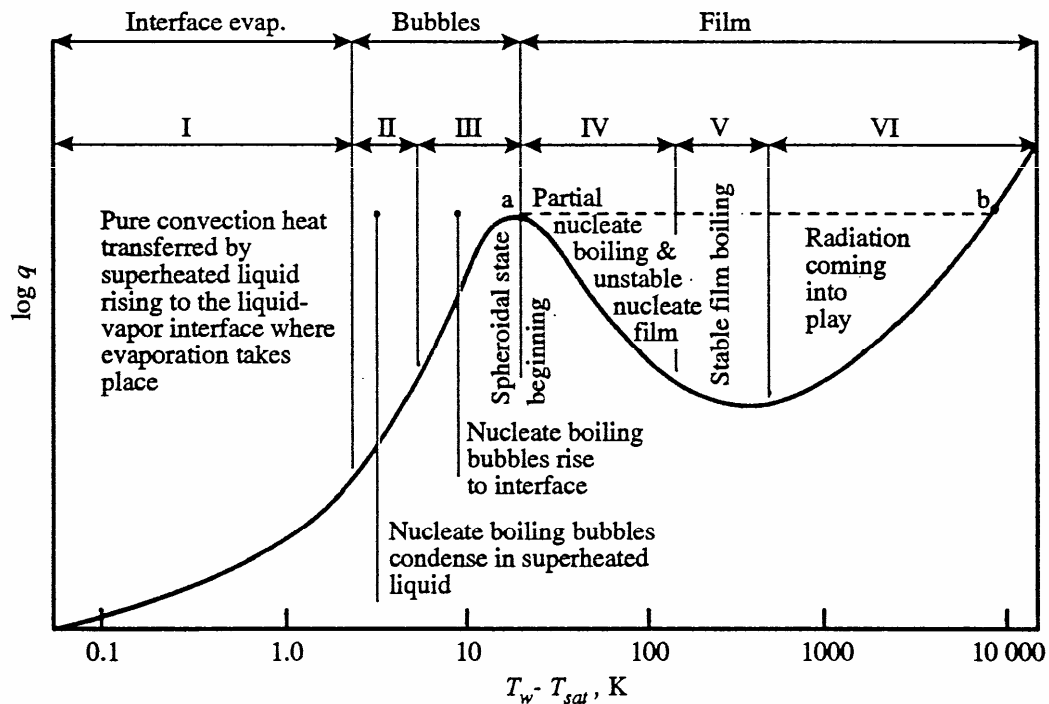


Figure 2.13 – Characteristic Boiling Curve [14]

Another way to determine the temperature profile is to define the surface temperature as a function of time. The S-shape portion of the idealized cooling curve in Figure 2.8 may be described by a function of the following form

$$T(R,t) = \frac{a-d}{1+(t/c)^b} + d \dots [16]$$

and fed directly into the solver.

---

It is clear that quenching is a critical part of the heat treatment process for aluminum alloys. The quench conditions can be varied greatly by changing the quenchant, quenchant temperature, agitation level, percent glycol, surface condition, section size, etc. The properties can be calculated based on Quench Factor Analysis. Temperature and stress profiles can be calculated. Reduction in residual stress trends with reduction in mechanical properties. The quench process is typically a compromise between the residual stress and mechanical properties. The next step is to calculate the attainable mechanical properties for an idealized quench process that results in no residual stress and no compromise.

### **3.0 PROCEDURE**

Determination of quench rate limits that border on plastic deformation requires a knowledge and understanding of the factors that enter into thermal stress analysis. Those factors pertain to the physical properties of the subject alloy and to the shape, but not to the quench environment. Once those limits are known, then the quench environment can be tailored to approach the known limits.

The alloy's physical properties are temperature dependent, making analytical calculations impossible without relying on some approximations of linearity or constancy of properties. Numerical calculation methods allow all properties to vary with temperature in any fashion, albeit without the reward of a leverageable analytical equation. Euler's explicit finite-difference method, one of many methods suitable to the task, can be used to calculate the temperature profile as developed over time and the resultant instantaneous thermal stresses at each time step during quench simulation.

The physical properties of heat treatable aluminum alloys, unfortunately, do not depend solely on instantaneous temperature. If the quench is sufficiently quick to freeze the supersaturated condition and prevent a significant amount of solute from precipitating, it will be allowable to ignore the effects of precipitation on the physical properties during the quench. If not, the quench cannot be considered successful and minimum mechanical properties may not be met after aging. This study, therefore, ignores physical property variations beyond those dependent on instantaneous temperature. The physical properties data for aluminum alloy 7075 (W temper) used for the thermal stress calculations were supplied by Worcester Polytechnic Institute's Center for Heat Treat Excellence (CHTE). Data for the following properties [17] were fitted to

functions of temperature for use in the quench simulation as shown in Figures 3.1 through 3.6.

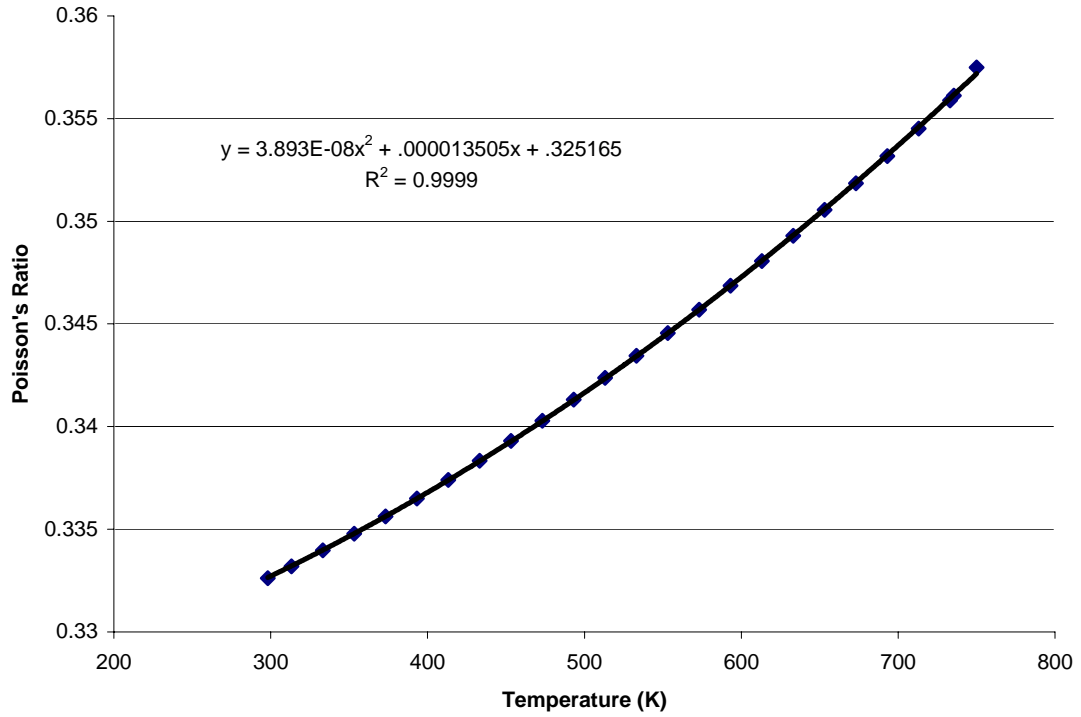


**Figure 3.1 – AA7075 – Poisson's Ratio v. Temperature**

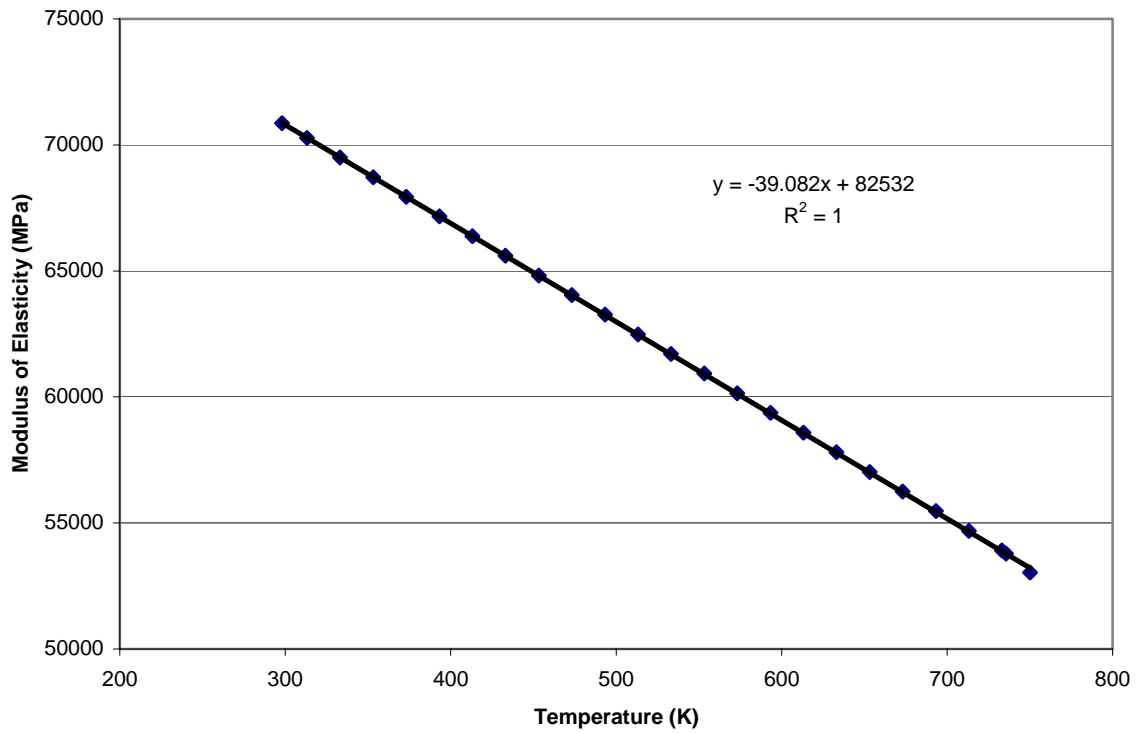


**Figure 3.2 – AA7075 - Modulus of Elasticity (Young’s Modulus) v. Temperature**

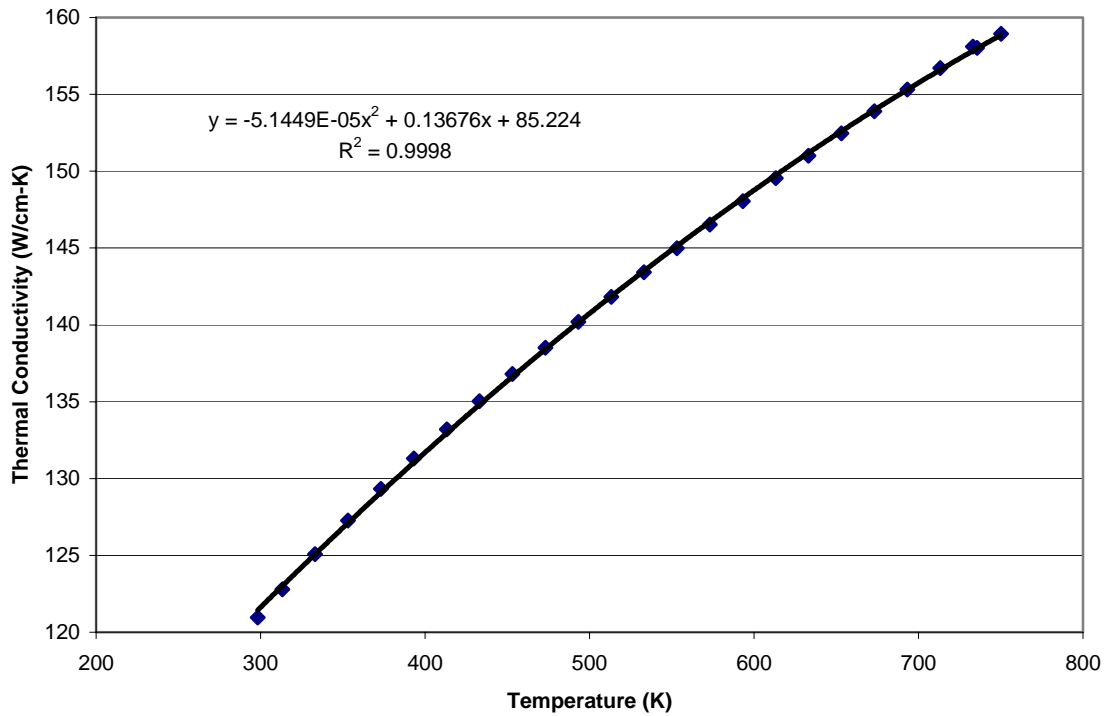


**Figure 3.3 – AA7075 - Thermal Conductivity v. Temperature**

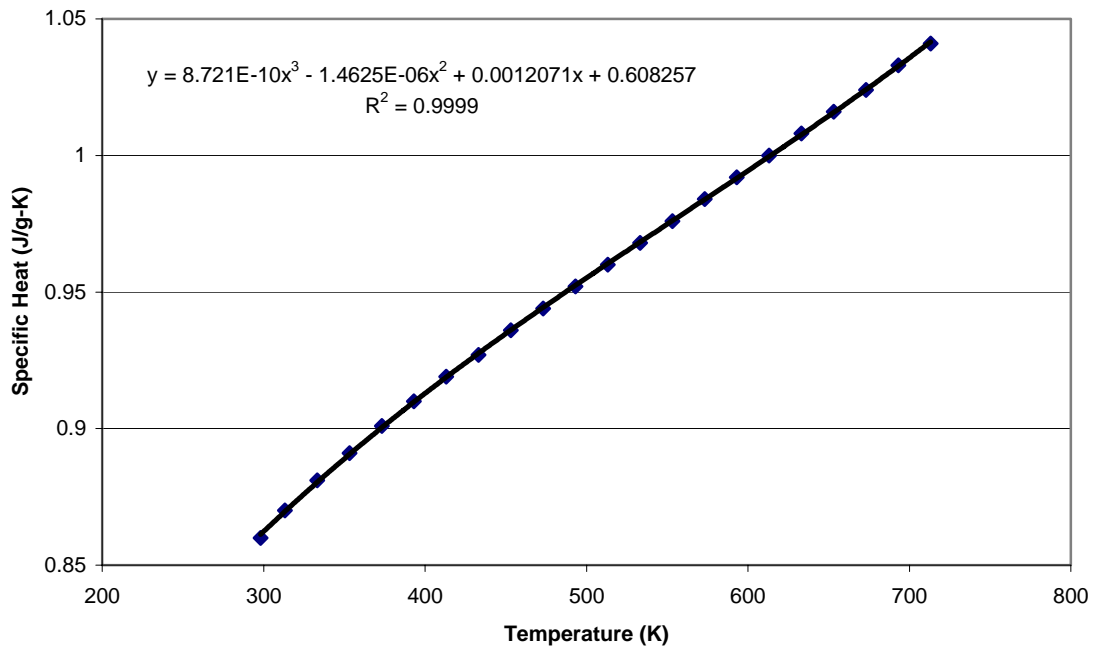


**Figure 3.4 – AA7075 – Specific Heat v. Temperature**

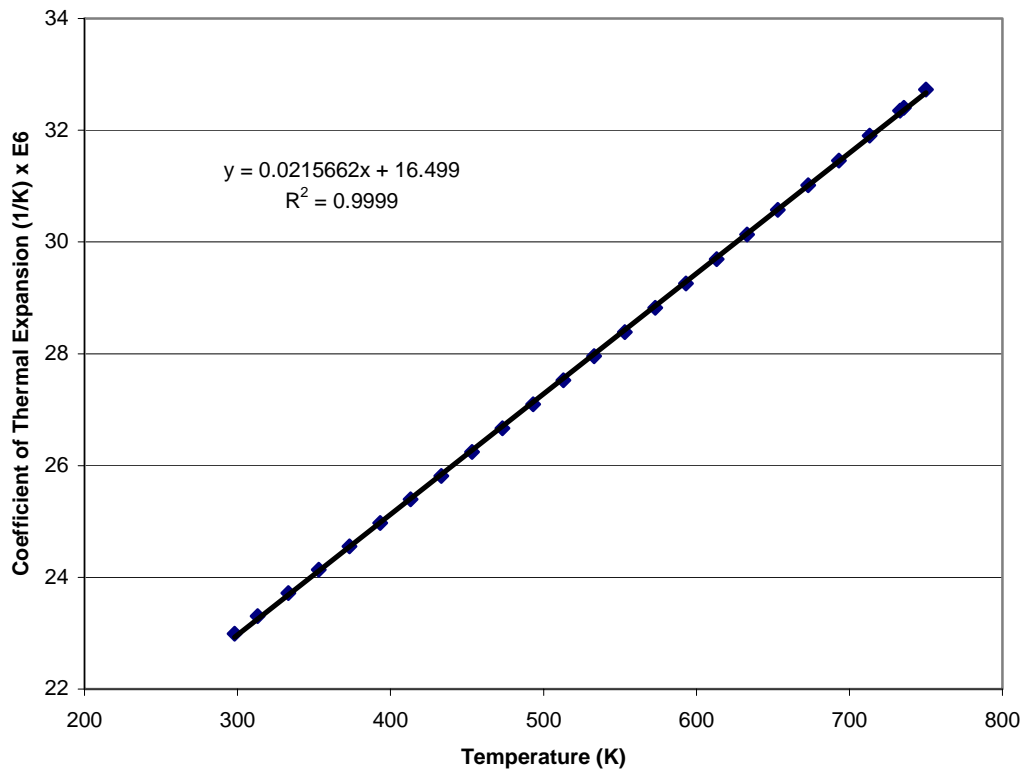


**Figure 3.5 – AA7075 – Coefficient of Thermal Expansion**

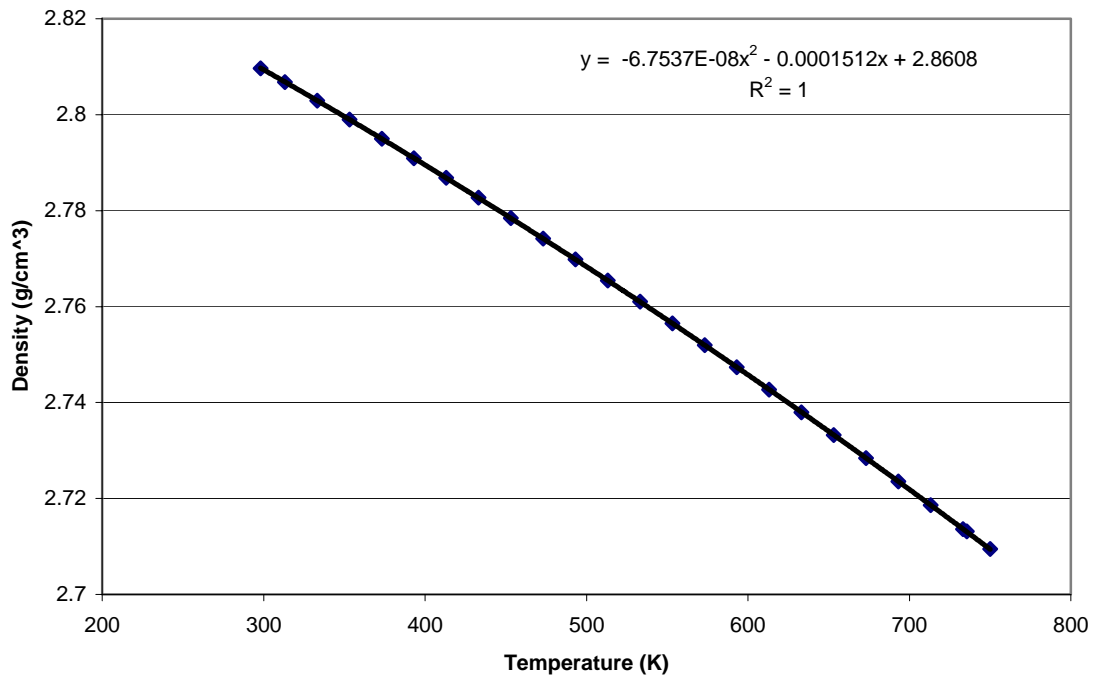


**Figure 3.6 – AA7075 – Density v. Temperature**

The following analysis assumes constant density because nodal displacements due to thermal expansion completely account for density variation because there are no phase transformations during cooling. It would be needless to account for both and gain nothing. The following calculation is provided as evidence:

$$\text{Density (hot)} = (\text{CTE} \cdot \Delta T + 1)^3 * \text{Density (cold)}$$

$$2.81 = ((27\text{E-}6/\text{K} * 450\text{K}) + 1)^3 * 2.71$$

Thermal stresses must never exceed the yield strength during the quench if plastic deformation is to be avoided. The 0.2% offset yield strength used as the yield criterion (also a function of temperature) that limits the quench rate is for the O temper (annealed) as data for W temper yield strength of 7075 aluminum alloy is not publicly available. Calculated quench rate limits will be slightly conservative because the yield strength of W temper should be higher than that of O temper for any temperature. The author argues

that the solid solution state would have higher yield strength than that of a solute depleted state with large, widely spaced precipitates. This error opposes that caused by using the available 0.2% yield strength data versus the subjective actual (lower) yield strength.

As mentioned earlier, quench calculations depend on shape. Aluminum alloy forgings come in a wide variety of configurations, but three shapes a) the infinite plate, b) the infinitely long cylinder and c) the sphere, offer the opportunity to reduce calculations to a single physical dimension while still representing a three dimensional shape. The infinitely long cylinder (with unrestrained ends) was chosen as the studied shape.

The analysis proposed by the author, whereby physical maximum quench rate limits are calculated, consists of three distinct algorithms: temperature, stress and quench factor analysis. As temperature profiles change during the quench, the elastic stress state is found at various time increments. Effective surface stress is then compared with the yield strength associated with the surface temperature. The convective heat transfer coefficient 'h' is increased only when the yield strength exceeds the surface stress. In this way, heat transfer during quench simulation is controlled by error. The time step allowed by Euler's method combined with the small amount by which 'h' is allowed to increase at each time step, prevents significant error. After quench completion, time-temperature data is used to calculate the quench factor and resultant yield strength for each node. The analysis produces a nodal time-temperature history for 2" diameter bar as shown in Figure 3.7. The rate of temperature drop increases as the surface cools.

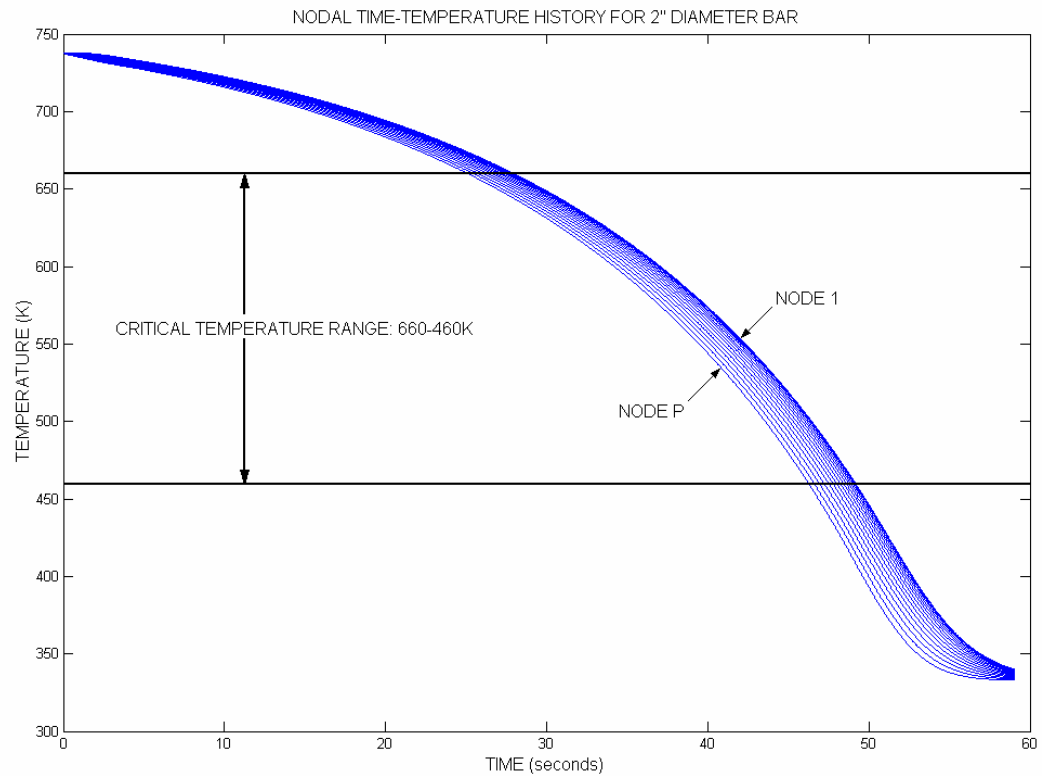


**Figure 3.7 – Nodal Cooling Curve, Ø2” Bar, at Elasticity Limit**

Figure 3.8 shows how the surface stress is forced to chase surface yield strength until the allowed (programmed) rate of increase of ‘h’ can no longer keep pace with the increase in surface strength. By that time, the quench factor has stopped changing significantly. The fact that ‘h’ only varies with stress means that the quench environment has no bearing on the analysis. The solution, therefore, is independent of all process parameters and is only dependent on alloy and diameter. For example, if the quenchant temperature were different, the value of ‘h’ would change accordingly so as to equilibrate the surface stress and surface yield strength at each time step. The value of ‘h’ matters only in that it serves to highlight the fact that increasing amounts of heat may be extracted from the part surface as the surface cools and gains strength, and that

convective cooling must accelerate through the critical temperature range. Figure 3.8 illustrates how surface thermal stress is forced to match surface yield strength over the critical cooling range. Figure 3.9 plots 'h' for the same simulation. It shows that the surface heat transfer need not exceed approximately  $.25\text{W}/\text{cm}^2$  (which is a heat transfer rate common in quenching aluminum.)

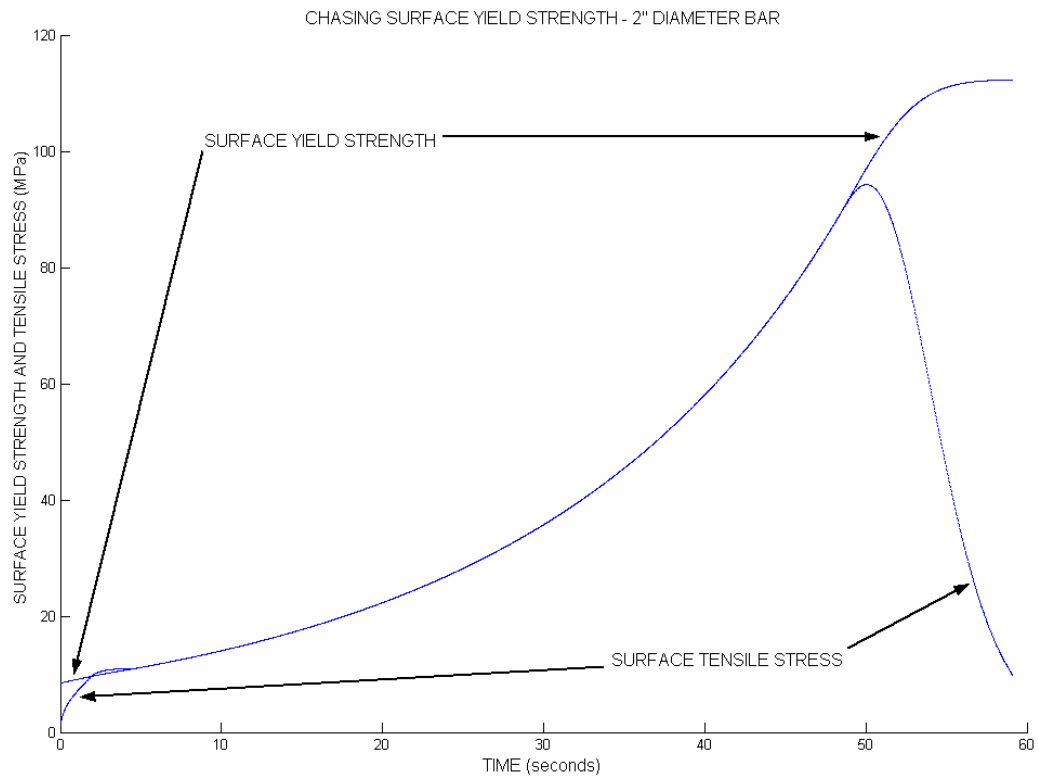


**Figure 3.8 – Chasing Elasticity Limit with Thermal Stress**

The critical temperature range shown in Figure 3.7 is the range in which approximately 99% of the quench factor is generated. It serves to illustrate that surface tensile stresses match surface yield strength in Figure 3.8 during the period (25-50s) in which temperature is falling through the critical range.

Using the foregoing hypothesis, Quench Factor Analysis of several bar diameters is shown for temper T73 in Figure 3.10. A graph of resultant yield strength is given in

Figure 3.11. The results show that quenching 7075 bar without incurring plastic strain can only occur at diameters of 2" or less. Quench factor analysis accuracy degrades beyond the 15% property loss level. For the purposes of this analysis, however, the concept remains valid.

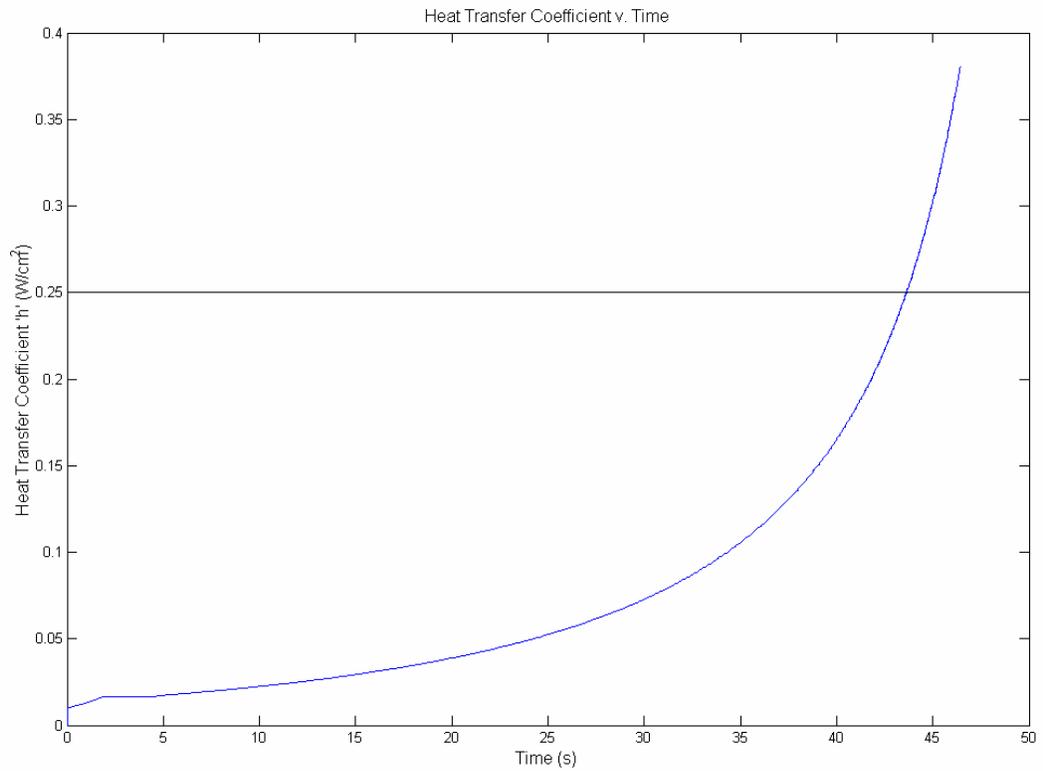


**Figure 3.9 – Elastic Limit Heat Transfer Coefficient v. Time**

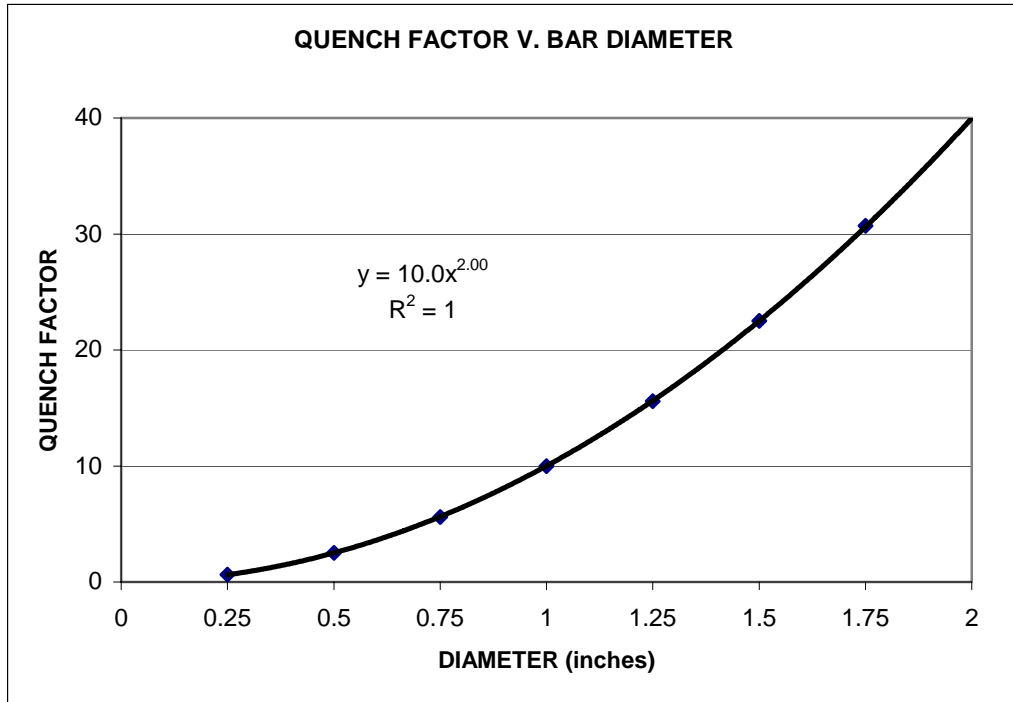


**Figure 3.10 – Elastic Limit Quench Factor v. Bar Diameter**

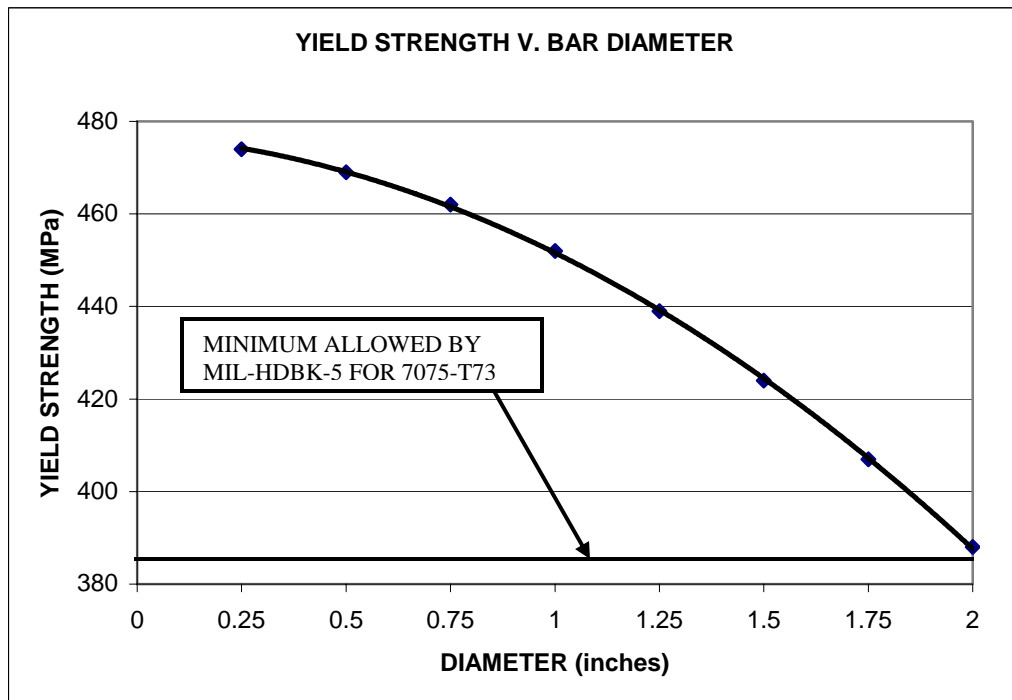


**Figure 3.11 – Elastic Limit Yield Strength v. Bar Diameter**

For comparison, heat transfer coefficients for boiling water quench and room temperature quench were fed into the simulation program. For boiling water quench, the effective heat transfer coefficient in the critical temperature range is approximately constant at  $h = .05 \text{ W/cm}^2$  regardless of agitation level. For room temperature quench, the heat transfer coefficient, at high agitation level, is approximately linear at  $h = .0005T + .15 \text{ W/cm}^2$ , where T is in Celsius. [15] The simulations assume purely elastic behavior even though the elastic limits are exceeded. Figures 3.12 and 3.13 show the simulation results. Quench factors ( $\tau$ ) for boiling water and room temperature quench are 144 and 19, respectively. Comparing simulations reveals that room temperature quench causes severe plastic strain (and high residual stress) while boiling water quench produces only mild plastic strain (and low residual stress). Note that boiling water quench will not produce minimum mechanical properties with a quench factor of 144.

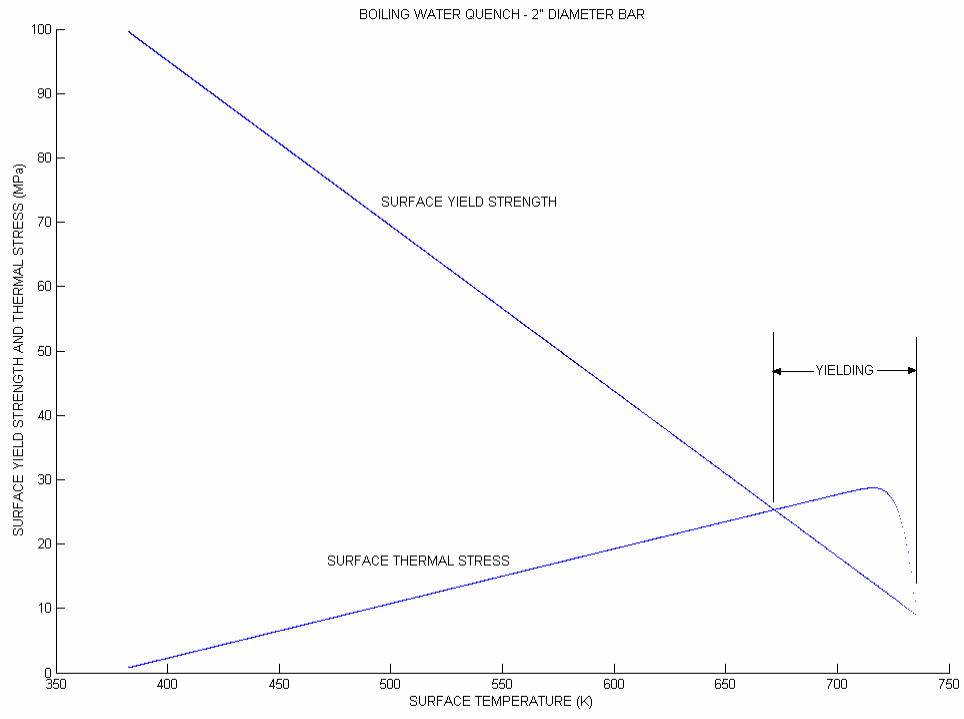


**Figure 3.12 – Boiling Water Quench Simulation**

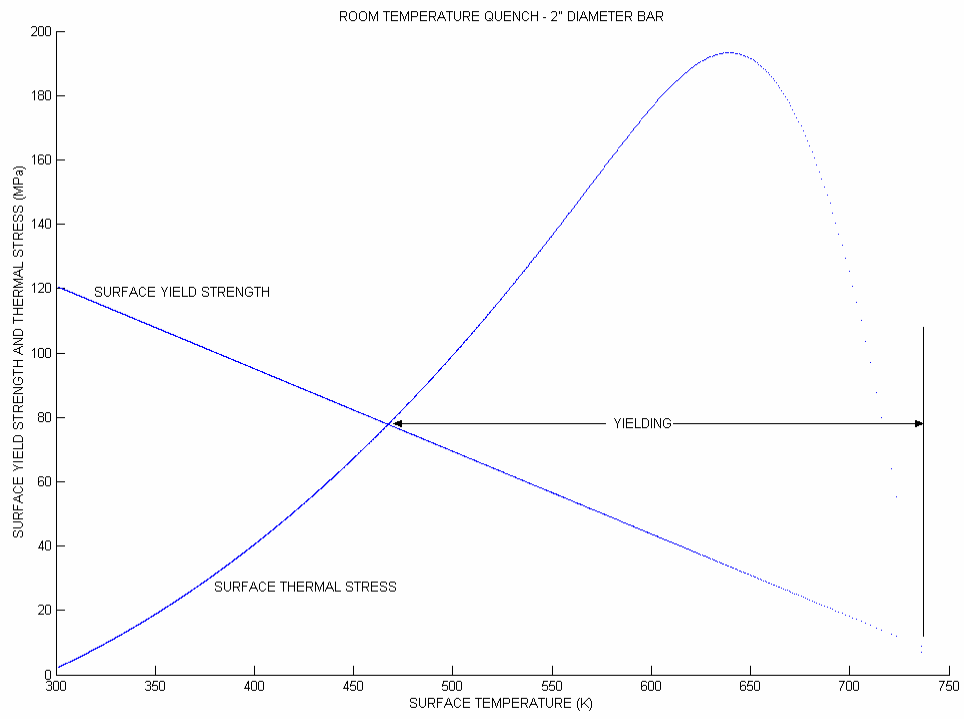


**Figure 3.13 – Room Temperature Quench Simulation**

#### 4.0 PROGRAM DESCRIPTION

The program is divided into four sections: input & initialization, solution of the temperature profile at each time increment, solution of the surface thermal stress, and Quench Factor Analysis. Figure 4.1 depicts program flow.

**Input and Initialization:** Sets the number of nodes, the initial heat transfer coefficient, constant density, initial constant temperature distribution, the ambient quenchant temperature (which is immaterial as long as it is well below the bottom of the C-curve), the simulation stop temperature at node 1, and the bar diameter. All counters and matrices are initialized as well.

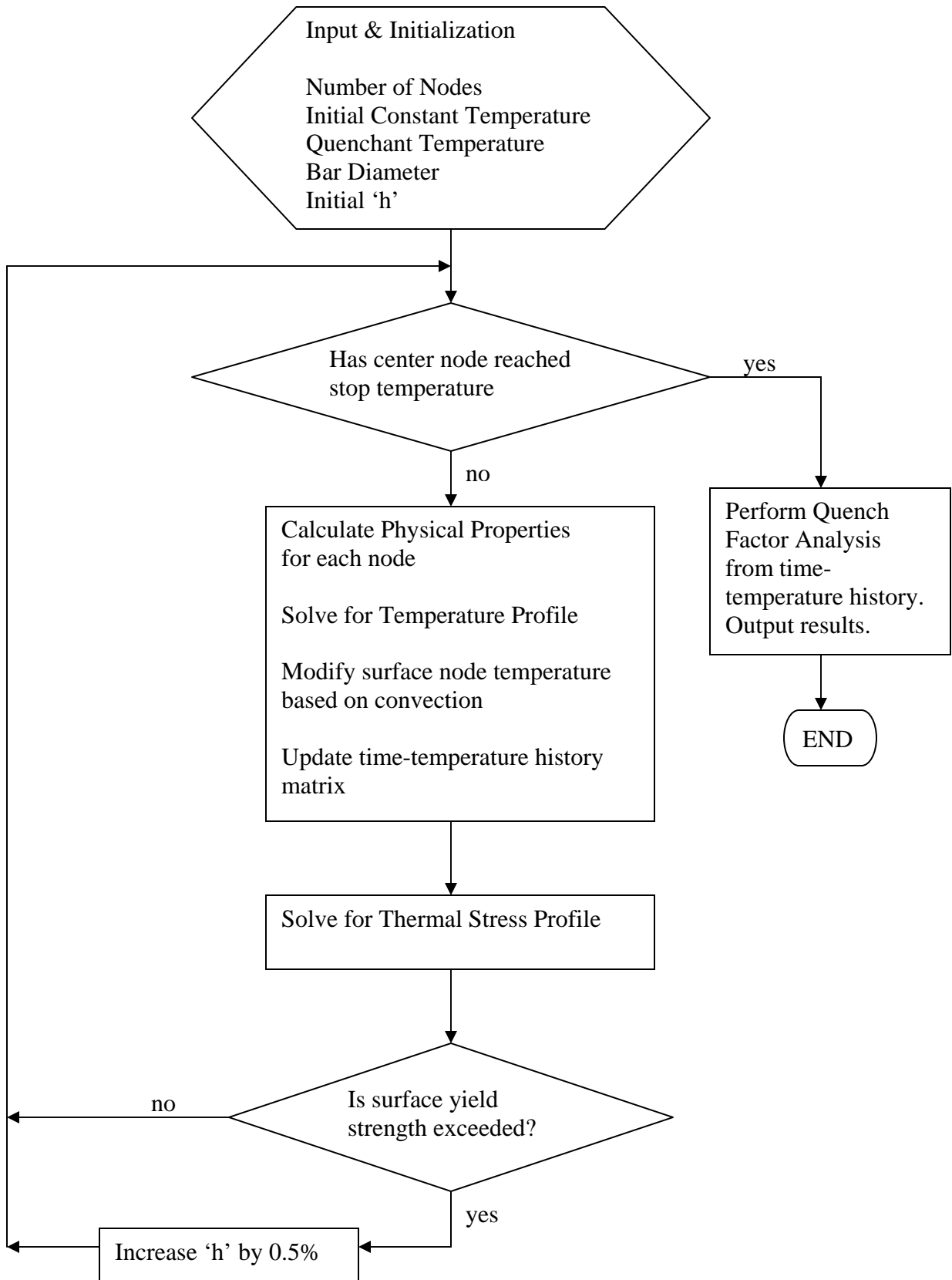
**Temperature Profile:** The main loop is initiated and continues until the stop temperature is reached at node 1. Based on the current temperature profile and functions of the material properties, the thermal conductivity, specific heat and thermal diffusivity are calculated at the positive and negative half-steps of each node. The time step and the values of  $\Theta$  are found for each node. Next, the matrix of coefficients (relaxation matrix) is set up using the equations found in Appendix B and the new temperature profile is found. At this time, the surface node temperature is updated based on the effect of surface convection that changes with current surface temperature, heat transfer coefficient ( $h$ ) and specific heat. The time-temperature history matrix is appended with the entire temperature profile, plus a row to record the real time and a row to record  $h$ .

**Surface Thermal Stress:** This section solves the simultaneous stress equilibrium and compatibility equations found in Appendix A. Because the temperature profile is known, the stress state at any node may be found. Only the stress at the surface node matters because this will always be the location of highest stress (highest thermal

gradient during continuous cooling) and the comparison between the surface stress and the surface yield strength will determine if  $h$  is allowed to increase at the next time step. Here, matrices for Poisson's ratio, coefficient of thermal expansion, yield strength, and a modified elastic modulus are calculated by plugging the elements of the nodal temperature profile into the associated functions of temperature. The solver computes the stress state at each node. Finally, the surface stress is compared to the surface yield strength. If the yield strength is not exceeded,  $h$  is allowed to increase by 0.5%. If not,  $h$  remains the same. The loop runs again for the next time increment, temperature profile and stress state.

Quench Factor Analysis: Based on the time-temperature history and the method shown in Figure 2.5, the Quench Factor and resultant yield strength for each node is calculated. Output includes the values of  $\tau$  and yield strength at each node and the complete time-temperature plot showing the cooling curve for each node.

**Figure 4.1 – Program Flowchart**



## 5.0 CONCLUSIONS

It is theoretically possible to quench aluminum alloy 7075 bar up to 2" diameter without inducing residual stress and exceed the minimum design strength. Heat transfer coefficients beyond  $.25\text{W}/\text{cm}^2$  are not critical to a successful quench. At the elastic limit, the quench factor varies with bar diameter according to the following equation:

$$\tau = 10D^2$$

where D is the bar diameter. This translates into a quench factor of 40 for 2" bar.

The theoretical cooling curves at the elastic limit accelerate from a very slow rate of heat transfer at the start of quench to a rate that is normally achievable using standard quench practices. Controlling heat flux based on the temperature profile so that the surface yield strength is not exceeded by the surface thermal stress may provide the practical answer.

## **6.0 RECOMMENDATIONS FOR FUTURE WORK**

The initial slow cooling required to avoid plastic strain may cause errors in Quench Factor Analysis. A non-isokinetic QFA model was developed by Staley and Tiryakoglu to account for slow cooling in the upper portion of the C-curve. This method extends QPA property prediction accuracy from approximately 15% to 70% reduction in properties. [18]

Slow cooling may also cause significant solute precipitation and vacancy migration so as to affect the yield strength versus temperature relation during quench. Incorporation of this effect in the simulation would be beneficial.

An investigation into the effects of thermal shock (strain rate sensitivity) on the yield strength may prove useful.

Specialized equipment would be required to generate smoothly accelerated cooling as proposed. Experimentation is needed to produce the required quench conditions and to verify that results are closely predicted.

Stress corrosion resistance is measured by electrical conductivity. A C-curve for this property/alloy combination should be used to verify the proper stress corrosion resistance is attained when quenching as described here.

Scaling this concept to production will not be robust. The calculations used to determine the elastic limit quench curve ignore all quench process parameters, some of which will cause wide variation in quench rates and quench uniformity. Much experimentation must be done before any guidelines for the institution of this concept can be generated.

## 7.0 APPENDIX A – STRESS EQUATION DERIVATIONS

### STRESS EQUILIBRIUM

$$\frac{d}{dr}(r\sigma_r) - \sigma_\theta = 0$$

at the negative half - step,

$$\frac{d}{dr}(r\sigma_r)_{i-1/2} - \sigma_{\theta,i-1/2} = 0$$

$$\frac{r_i\sigma_{r_i} - r_{i-1}\sigma_{r,i-1}}{r_i - r_{i-1}} = \frac{\sigma_{\theta,i-1} + \sigma_{\theta,i}}{2}$$

$$(r_i)\sigma_{r_i} - \left(\frac{\Delta r}{2}\right)\sigma_{\theta,i} = (r_{i-1})\sigma_{r,i-1} + \left(\frac{\Delta r}{2}\right)\sigma_{\theta,i-1}$$

### STRESS - STRAIN RELATIONS

$$\varepsilon_r = \frac{1}{E}(\sigma_r - \nu\sigma_\theta - \nu\sigma_z) + \alpha T$$

$$\varepsilon_\theta = \frac{1}{E}(\sigma_\theta - \nu\sigma_r - \nu\sigma_z) + \alpha T$$

$$\varepsilon_z = \frac{1}{E}(\sigma_z - \nu\sigma_\theta - \nu\sigma_r) + \alpha T$$

rearrange  $\varepsilon_z$

$$\sigma_z = E(\varepsilon_z - \alpha T) + \nu\sigma_r + \nu\sigma_\theta$$

substitute in  $\varepsilon_\theta$

$$\varepsilon_\theta = \frac{1}{E}(\sigma_\theta - \nu\sigma_r - \nu(E(\varepsilon_z - \alpha T) + \nu\sigma_r + \nu\sigma_\theta)) + \alpha T$$

## COMPATIBILITY EQUATION

$$\frac{d}{dr} \varepsilon_{\theta} + \frac{\varepsilon_{\theta} - \varepsilon_r}{r} = 0$$

substitute  $\varepsilon_{\theta}, \varepsilon_r$

$$\frac{d}{dr} \left( \frac{1}{E} (\sigma_{\theta} - \nu \sigma_r - \nu (E(\varepsilon_z - \alpha T) + \nu \sigma_r + \nu \sigma_{\theta})) + \alpha T \right) = \frac{1}{rE} (\sigma_r - \sigma_{\theta} + \nu \sigma_r - \nu \sigma_{\theta})$$

taking  $\frac{d}{dr} (\nu \varepsilon_z) = 0$  as  $\frac{d\varepsilon_z}{dr} = 0$  in plane - strain and  $\frac{d\nu}{dr}$  is extremely small

$$\frac{d}{dr} \left( \left( \frac{1-\nu^2}{E} \right) \sigma_{\theta} - \left( \frac{\nu+\nu^2}{E} \right) \sigma_r + (1+\nu)\alpha T \right) = \frac{(1+\nu)}{rE} (\sigma_r - \sigma_{\theta})$$

substitute  $E' = \frac{E}{1+\nu}$  at the negative half - step

$$\frac{\frac{1-\nu_i}{E'_i} \sigma_{\theta,i} - \frac{1-\nu_{i-1}}{E'_{i-1}} \sigma_{\theta,i-1} - \frac{\nu_i}{E'_i} \sigma_{r,i} + \frac{\nu_{i-1}}{E'_{i-1}} \sigma_{r,i-1} + (1+\nu_i)\alpha_i T_i - (1+\nu_{i-1})\alpha_{i-1} T_{i-1}}{\Delta r} = \frac{\frac{\sigma_{r,i}}{r_i E'_i} + \frac{\sigma_{r,i-1}}{r_{i-1} E'_{i-1}} - \frac{\sigma_{\theta,i}}{r_i E'_i} - \frac{\sigma_{\theta,i-1}}{r_{i-1} E'_{i-1}}}{2}$$

substitute  $(i-1)\Delta r = r_i$

$$\left( \frac{1}{2E'_i(i-1)} + \frac{\nu_i}{E'_i} \right) \sigma_{r,i} - \left( \frac{-1}{2E'_i(i-1)} + \frac{1-\nu_i}{E'_i} \right) \sigma_{\theta,i} = \left( \frac{1}{2E'_{i-1}(i-2)} + \frac{\nu_{i-1}}{E'_{i-1}} \right) \sigma_{r,i-1} - \left( \frac{-1}{2E'_{i-1}(i-2)} + \frac{1-\nu_{i-1}}{E'_{i-1}} \right) \sigma_{\theta,i-1} + (1+\nu_i)\alpha_i T_i - (1+\nu_{i-1})\alpha_{i-1} T_{i-1}$$

The stress equilibrium and compatibility equations have the form

$$C\sigma_{r,i} + D\sigma_{\theta,i} = F\sigma_{r,i-1} + G\sigma_{\theta,i-1} + H$$

and must be solved simultaneously. The surface stress state gives the boundary

condition: The part surface is free so the radial stress there must be zero. [12]

## 8.0 APPENDIX B - TEMPERATURE EQUATION DERIVATIONS

FOURIER'S LAW OF HEAT CONDUCTION IN DIFFERENTIAL FORM

EXPRESSED AS HEAT FLUX PER UNIT AREA IN CYLINDRICAL FORM

$$q_r = -k \frac{\partial T}{\partial r}$$

ENERGY BALANCE:

HEAT IN – HEAT OUT = HEAT ACCUMULATION

FOR INTERNAL NODES  $i$ :

$$\left( Ak \frac{dT}{dr} \right)_{i-1/2} - \left( Ak \frac{dT}{dr} \right)_{i+1/2} = \rho \left( VC_p \frac{dT}{dt} \right)_i$$

$dr$  to be constant

$$2\pi \left( \frac{r_{i-1} + r_i}{2} \right) Lk^- \left( \frac{T_{i-1} - T_i}{\Delta r} \right) - 2\pi \left( \frac{r_{i+1} + r_i}{2} \right) Lk^+ \left( \frac{T_i - T_{i+1}}{\Delta r} \right) = \rho \left( \pi (r_{i+1/2}^2 - r_{i-1/2}^2) L \right) \left( C_p \frac{\Delta T}{\Delta t} \right)_i$$

$$\text{substitute } \alpha = \frac{k}{\rho C_p}$$

$$\alpha^- \frac{\Delta t}{\Delta r} (r_{i-1} + r_i) (T_{i-1} - T_i) - \alpha^+ \frac{\Delta t}{\Delta r} (r_{i+1} + r_i) (T_i - T_{i+1}) = \Delta r (r_{i+1/2} + r_{i-1/2}) \Delta T$$

$$\text{substitute } \Theta = \frac{\alpha \Delta t}{(\Delta r)^2}$$

$$\Delta T = \Theta^- (T_{i-1} - T_i) \left( \frac{r_{i-1} + r_i}{r_{i+1/2} + r_{i-1/2}} \right) - \Theta^+ (T_i - T_{i+1}) \left( \frac{r_{i+1} + r_i}{r_{i+1/2} + r_{i-1/2}} \right)$$

substitute  $(i-1)\Delta r = r_i$

$$T_i^{t+\Delta t} = T_i + \Theta^- (T_{i-1} - T_i) \left( \frac{(i-2) + (i-1)}{(i-1/2) + (i-3/2)} \right) - \Theta^+ (T_i - T_{i+1}) \left( \frac{(i) + (i-1)}{(i-1/2) + (i-3/2)} \right)$$

$$T_i^{t+\Delta t} = T_{i-1} \left[ \Theta^- \left( \frac{i-3/2}{i-1} \right) \right] + T_i \left[ 1 - \Theta^- \left( \frac{i-3/2}{i-1} \right) - \Theta^+ \left( \frac{i-1/2}{i-1} \right) \right] + T_{i+1} \left[ \Theta^+ \left( \frac{i-1/2}{i-1} \right) \right]$$

FOR AXIS NODE  $i = 1$

$$\begin{aligned}
0 - \left( Ak \frac{dT}{dr} \right)_{3/2} &= \rho \left( VC_P \frac{dT}{dt} \right)_1 \\
- 2\pi \left( \frac{\Delta r}{2} \right) L k^+ \left( \frac{T_1 - T_2}{\Delta r} \right) &= \rho \pi \left( \frac{\Delta r}{2} \right)^2 L \left( C_P \frac{\Delta T}{\Delta t} \right)_1 \\
- \alpha^+ (T_1 - T_2) &= \left( \frac{\Delta r}{2} \right)^2 \left( \frac{\Delta T}{\Delta t} \right)_1 \\
\Delta T &= \frac{4\alpha^+ \Delta t}{(\Delta r)^2} (T_2 - T_1) \\
T_1^{t+1} &= T_1 [1 - 4\Theta^+] + T_2 [4\Theta^+]
\end{aligned}$$

FOR SURFACE NODE  $i = N + 1 = P$

$$\begin{aligned}
\left( Ak \frac{dT}{dr} \right)_{P-1/2} - (AhdT)_P &= \rho \left( VC_P \frac{dT}{dt} \right)_P \\
2\pi \left( \frac{r_{P-1} + r_P}{2} \right) L k^- \left( \frac{T_{P-1} - T_P}{\Delta r} \right) - 2\pi r_P L h (T_P - T_\infty) &= \rho \pi (r_P^2 - r_{P-1/2}^2) L \left( C_P \frac{\Delta T}{\Delta t} \right)_P \\
\Delta T &= 2 \left( \frac{r_{P-1} + r_P}{2} \right) k^- \left( \frac{T_{P-1} - T_P}{\Delta r} \right) \frac{\Delta t}{\rho C_P \frac{\Delta r}{2} (r_P + r_{P-1/2})} - 2r_P h (T_P - T_\infty) \frac{\Delta t}{\rho C_P \frac{\Delta r}{2} (r_P + r_{P-1/2})} \\
\Delta T &= \frac{2\alpha^- \Delta t}{(\Delta r)^2} (T_{P-1} - T_P) \frac{r_{P-1} + r_P}{r_P + r_{P-1/2}} - \frac{2h\Delta t}{\rho C_P \frac{\Delta r}{2}} (T_P - T_\infty) \frac{r_P}{r_P + r_{P-1/2}} \\
\Delta T &= 2\Theta^- (T_{P-1} - T_P) \frac{(N-1) + N}{N + (N-1/2)} - \frac{4h\Delta t}{\rho C_P \Delta r} (T_P - T_\infty) \frac{N}{N + (N-1/2)} \\
\Delta T &= 2\Theta^- (T_{P-1} - T_P) \frac{N-1/2}{N-1/4} - \frac{4h\Delta t}{\rho C_P \Delta r} (T_P - T_\infty) \frac{N}{2N-1/2} \\
T_P^{t+1} &= T_{P-1} \left[ 2\Theta^- \left( \frac{N-1/2}{N-1/4} \right) \right] + T_P \left[ 1 - 2\Theta^- \left( \frac{N-1/2}{N-1/4} \right) \right] + (T_\infty - T_P) \frac{4h\Delta t}{\rho C_P \Delta r} \left( \frac{N}{2N-1/2} \right)
\end{aligned}$$

## 9.0 APPENDIX C - MATLAB Program

```

% TEMPERATURE PROFILE axi-symmetric
clear all
figure
hold on;

% inputs
N = 16;% number of divisions (#nodes-1)
h = .01;% INITIAL heat transfer coefficient W/cm^2K
rho = 2.76;% density g/cm^3
T0 = 738;% initial temperature distribution K // 738K = 870F
ambient = 333;% 333K = 140F ...ambient temperature K
stoptemp = 340;% K
R = 1*2.54;% bar radius in cm

% initialize
P = N+1;% number of nodes
C1 = zeros(P,P);% matrix of coefficients
T = T0*ones(P,1);% initial temperature distribution (constant) K
G = zeros(P+2,1);% temperature history...P+1 is time stamp...P+2 is 'h'
G(1:P) = T;
dr = R/N;
sumtime = 0;% real time counter
iter = 0;% step counter

% -----
while T(1) >= stoptemp
iter = iter + 1;

% thermal variables
for i = 1:N
aveT = (T(i) + T(i+1))/2;% average nodal temperature
kp(i) = -5.1449E-07*aveT^2 + .0013676*aveT + .85224;% thermal conductivity k(T) W/cmK
cp(i) = 8.721E-10*aveT^3 - 1.4625E-06*aveT^2 + 0.0012071*aveT + 0.608257;% specific
heat Cp(T) J/gK
ap(i) = kp(i)/(rho*cp(i));% thermal diffusivity alpha(T) cm^2/s
an(i+1) = ap(i);
end
cp(P) = 8.721E-10*T(P)^3 - 1.4625E-06*T(P)^2 + 0.0012071*T(P) + 0.608257;

% time step
tp(N) = .4;
tn(P) = tp(N);
dt = tp(N)*dr^2/an(P);
sumtime = sumtime + dt;

% compute theta's
Z = dt/(dr^2);
for j = 1:N-1;
tp(j) = ap(j)*Z;
tn(j+1) = an(j+1)*Z;
end

% obtain matrix and solve
C1(1,2) = 4*tp(1);
C1(1,1) = 1 - C1(1,2);
for k = 2:N
C1(k,k-1) = tn(k)*(k-1.5)/(k-1);
C1(k,k+1) = tp(k)*(k-.5)/(k-1);
C1(k,k) = 1 - C1(k,k-1) - C1(k,k+1);
end
C1(P,N) = 2*tn(P)*(N-.5)/(N-.25);
C1(P,P) = 1 - C1(P,N);

T = C1*T;
T(P) = T(P) + (ambient-T(P))*2*h*dt*N/(rho*cp(P)*dr*(N-.25));% convection effect
G = [G [T; sumtime; h]];% update nodal temperature history including timestamp, h

```

```

% -----
% FINITE DIFFERENCE axi-symmetric elastic plain-strain stress
% CONSTANT dr
% VARIABLE E, CTE, v

% initialize
L = zeros(2,2,P);
M = zeros(2,P);
A = zeros(2,2,P);
A(1,1,1) = 1;
A(2,2,1) = 1;
B = zeros(2,P);
S = zeros(2,P);

% GENERATE v, E, CTE, YS MATRICES
v = 3.893E-08*T.^2 + .000013505*T + .325165;
E = (-39.082*T + 82532)./(1 + v);% modified E (div by 1+v) in MPa
CTE = .0215662E-6*T + 16.499E-6;% /K
YS = -.2567*T + 197.7762;% MPa YS = (-37.224*T + 28684)*.006895

D = .5;
F = 0;
FF = 0;
GG = 0;
HH1 = CTE(1).*T(1).*(v(1)+1);

% solver
for k = 2:P;
C = k-1;
a = 1/(2*(C)*E(k));
CC = v(k)/E(k) + a;
DD = (1-v(k))/E(k) + a;
HH2 = CTE(k).*T(k).*(v(k)+1);
HH = HH2 - HH1;
denom = C*DD - CC*D;
L(:, :, k) = [(DD*F - D*FF) (DD*D + D*GG) ; (CC*F - C*FF) (CC*D + C*GG)]./denom;
M(:, k) = [-HH*D ; -HH*C]./denom;
A(:, :, k) = L(:, :, k)*A(:, :, C);
B(:, k) = L(:, :, k)*B(:, C) + M(:, k);
F = C;
FF = CC - 2*a;
GG = DD - 2*a;
HH1 = HH2;
end

s = -B(1,P)/(A(1,1,P) + A(1,2,P));
S(:,1) = [s ; s];

for j = 2:P;
S(:,j) = A(:, :, j)*S(:,1) + B(:, j);
end

plot (sumtime,S(2,P));
plot (sumtime,YS(P));

if YS(P)>=S(2,P)
h = 1.005*h;
end

% -----
end

% TIME-TEMPERATURE PLOT
figure
for p = 1:P
plot (G(P+1,:),G(p,:))
hold on
end

sumtime% real time duration

```

```

% -----
% QUENCH FACTOR ANALYSIS for 7075 aluminum
% takes time-temp history and calculates theoretical strength for each node

k1 = -.005013;% ln(99.5%) (fraction transformed)
k2 = 1.37E-13;% seconds (1/nucleation sites)
k3 = 1069;% J/mol
k4 = 737;% K solvus temp
k5 = 137000;% J/mol activation energy for diffusion
gc = 8.31441;% J/mol-K gas constant
my = 475;% MPa maximum yield strength

c1 = -k1*k2;
c2 = k3*k4^2/gc;
c3 = k5/gc;
deltat = G(P+1,2:iter+1) - G(P+1,1:iter);
deltat = [0 deltat];
CT = G(1:P,:);
for row = 1:P;
    for col = 1:iter+1;
        CT(row,col) = exp(c2/CT(row,col)/(k4-CT(row,col))^2) * exp(c3/CT(row,col));
    end
end
CT = c1.*CT;

q = CT;
for row2 = 1:P;
    q(row2,:) = deltat./q(row2,:);
    tau(row2) = sum(q(row2,:));
    yield(row2) = my*exp(k1*tau(row2));
end

tau
yield

```

## 10.0 REFERENCES

1. "Heat Treating of Aluminum Alloys," *ASM Handbook Vol. 4: Heat Treating*. 1991, ASM International, Materials Park, OH. p841-879.
2. Nock, Jr. J.A. "Properties of Commercial Wrought Alloys," *ALUMINUM Vol. I - Properties, Physical Metallurgy and Phase Diagrams*. 1967, ASM, Metals Park, OH. p303-336.
3. "Metallic Materials and Elements for Aerospace Vehicle Structures," *Military Standardization Handbook*, Vol. 5D. June 1983.
4. Hunsicker, H.Y. "The Metallurgy of Heat Treatment," *ALUMINUM Vol. I - Properties, Physical Metallurgy and Phase Diagrams*. 1967, ASM, Metals Park, OH. p109-162.
5. Evancho, J.W. and Staley, J.T. "Kinetics of Precipitation in Aluminum Alloys During Continuous Cooling," *Metallurgical Transactions A*, Vol. 5A, January 1974. p43-47.
6. Totten, G.E., Webster, G.M. and Bates, C.E., *Proceedings of the 1<sup>st</sup> International Non-Ferrous Processing and Technology Conference*, March 1997. p303-313.
7. Barker, R.S. and Sutton, J.G. "Stress Relieving and Stress Control," *ALUMINUM Vol. III - Fabrication and Finishing*. 1967, ASM, Metals Park, OH. p355-382.
8. Bates, C.E. "Selecting Quenchants to Maximize Tensile Properties and Minimize Distortion in Aluminum Parts," *J. Heat Treat.* Vol. 5 (No. 1). 1987. p27-40
9. Dolan, G.P., Robinson, J.S. and Morris, A.J. "Quench Factors and Residual Stress Reduction in 7175-T73 Plate," *Proceedings From Materials Solutions Conference*. November 2001, ASM International, Indianapolis, IN. p213-218.
10. Poirier, D.R. and Geiger, G.H. "Transport Phenomena in Materials Processing," TMS, Warrendale, PA, 1994. p266.
11. Croucher, T. "Critical Parameters for Evaluating Polymer Quenching of Aluminum," *J. Heat Treat.* Vol. 19 (No. 12). December 1987. p21-25.
12. Manson, S.S. "Thermal Stress and Low-Cycle Fatigue," McGraw-Hill Book Company, New York, 1966. p7-85.
13. [8] p571-610.
14. Rohsenow, W.M. "Developments in Heat Transfer," MIT Press, Cambridge, MA, 1964. Chapter 8.
15. Fontecchio, M. "Quench Probe and Quench Factor Analysis of Aluminum Alloys in Distilled Water," Master's Thesis, WPI, May 2002.
16. Jahanian, S. "A Numerical Study of Quenching of an Aluminum Solid Cylinder," *Journal of Thermal Stresses* Vol. 19. 1996. p513-529.
17. Data from Worcester Polytechnic Institute, Center for Heat Treat Excellence.
18. Staley, J.T and Tiryakoglu, M. *Proceedings, Materials Solution Conference*, ASM International, 2001. p6-14.